



Organic carbon and microbial activity in marine sediments on a global scale throughout the Quaternary

Douglas E. LaRowe^{a,*}, Sandra Arndt^b, James A. Bradley^{c,d}, Ewa Burwicz^e,
Andrew W. Dale^e, Jan P. Amend^{a,f}

^a Department of Earth Sciences, University of Southern California, Los Angeles, CA, USA

^b Department of Geosciences, Environment and Society, Free University of Brussels, Brussels, Belgium

^c School of Geography, Queen Mary University of London, Mile End Road, London E1 4NS, United Kingdom

^d Interface Geochemistry, GFZ German Research Centre for Geosciences, 14473 Potsdam, Germany

^e GEOMAR Helmholtz Centre for Ocean Research Kiel, Germany

^f Department of Biological Sciences, University of Southern California, Los Angeles, CA, USA

Received 31 January 2019; accepted in revised form 9 July 2020; Available online 28 July 2020

Abstract

Microbial degradation of organic carbon in marine sediments is a key driver of global element cycles on multiple time scales. However, it is not known to what depth microorganisms alter organic carbon in marine sediments or how microbial rates of organic carbon processing change with depth, and thus time since burial, on a global scale. To better understand the connection between the dynamic carbon cycle and life's limits in the deep subsurface, we have combined a number of global data sets with a reaction transport model (RTM) describing first, organic carbon degradation in marine sediments deposited throughout the Quaternary Period and second, a bioenergetic model for microbial activity. The RTM is applied globally, recognizing three distinct depositional environments – continental shelf, margin and abyssal zones. The results include the masses of particulate organic carbon, POC, stored in three sediment-depth layers: bioturbated Holocene (1.7×10^{17} g C), non-bioturbated Holocene (2.5×10^{18} g C) and Pleistocene (1.4×10^{20} g C) sediments. The global depth-integrated rates of POC degradation have been determined to be 1.3×10^{15} , 1.3×10^{14} and 3.0×10^{14} g C yr⁻¹ for the same three layers, respectively. A number of maps depicting the distribution of POC, as well as the fraction that has been degraded have also been generated. Using POC degradation as a proxy for microbial catabolic activity, total heterotrophic processing of POC throughout the Quaternary is estimated to be between 10^{-11} and 10^{-6} g C cm⁻³ yr⁻¹, depending on the time since deposition and location. Bioenergetic modeling reveals that laboratory-determined microbial maintenance powers are poor predictors of sediment biomass concentration, but that cell concentrations in marine sediments can be accurately predicted by combining bioenergetic models with the rates of POC degradation determined in this study. Our model can be used to quantitatively describe both the carbon cycle and microbial activity on a global scale for marine sediments less than 2.59 million years old. © 2020 Elsevier Ltd. All rights reserved.

Keywords: Reaction transport model; Deep biosphere; Microbial ecology; Organic carbon degradation; Quaternary; Bioenergetics; Reactive continuum model; Deep carbon; Holocene; Pleistocene

1. INTRODUCTION

Marine sediments consist of unconsolidated rock particles, organisms, volcanic debris, authigenic precipitates, cosmogenic deposits, water and organic carbon. They

* Corresponding author.

E-mail address: larowe@usc.edu (D.E. LaRowe).

constitute the uppermost layer of most oceanic crust and also blanket continental crust that lies under seawater. By covering 3.6×10^8 km² (Eakins and Sharman, 2010), they comprise one of the largest features of Earth's surface and therefore one of its largest habitats and carbon reservoirs. The transformation of organic carbon in sediments not only sustains a massive biosphere, but in the most dynamic upper tens of centimeters of sediments, the microbial oxidation of organic carbon alters the saturation state of pore waters with respect to calcium carbonate minerals. This consequently affects carbonate burial, an important part of the Walker thermostat that keeps Earth's temperature within livable limits (Emerson and Bender, 1981; Walker et al., 1981). Furthermore, microbial oxidation of organic carbon in sediments drives Fe, Mn and S cycles, processes that influence ocean chemistry (e.g. Berner, 1980; Middelburg, 1989; Boudreau and Ruddick, 1991; Canfield, 1993; Tromp et al., 1995; Jørgensen and Kasten, 2006; Thullner et al., 2009). In addition, the (selective) microbial degradation of organic carbon throughout the sediment column can impact the various sets of isotopic, biogenic/authigenic mineral and biomarker data that are used to interpret paleoenvironmental records (Zonneveld et al., 2010; Wehrmann et al., 2013; Freitas et al., 2017). On geologic time scales, the microbial processing of organic carbon in marine sediments plays a major role in controlling levels of oxygen and CO₂ in the atmosphere (Rothman, 2002; Berner, 2006) and the amount of CH₄ that is stored in near-shore sediments (Burwicz et al., 2011; Wadham et al., 2013).

The fate of organic carbon in sediments, and therefore the degree to which it impacts global biogeochemical cycles, is a function of the rate at which it is deposited and the type of environment in which it is delivered. Although approximately half of POC delivered to sediments is oxidized by oxygen-consuming microorganisms (Jørgensen and Kasten, 2006), other organisms using NO₃⁻, SO₄²⁻ and Fe- and Mn- oxides as electron acceptors flourish, driving, S, N, Fe and Mn cycles. POC can also be fermented, reduced to CH₄, or, with increasing depth and temperature, converted abiotically into hydrocarbons. Despite the critical role that marine sediment POC has driving global biogeochemical cycles, estimates for the modern-day flux of POC to the seafloor vary considerably. A review of the literature reveals a factor of 40 between the lowest and highest global POC flux estimates, spanning 137 to 5739 Tg C yr⁻¹ (Burdige, 2007; Wallmann et al., 2012), though many report values in the middle of this range: 1784 or 3127 Tg C yr⁻¹ (Middelburg et al., 1997), 2308 Tg C yr⁻¹ (Jørgensen, 1983), 2616 Tg C yr⁻¹ (Smith and Hollibaugh, 1993). Similarly, although the delivery of POC to the ocean floor is known to vary geographically and temporally (e.g. Arndt et al., 2006, 2009; Wehrmann et al., 2013), organic deposition patterns are poorly constrained, especially on a spatially well-resolved basis.

Rates of microbial organic carbon degradation in marine sediments can vary by at least eight orders of magnitude across ocean basins (Middelburg, 1989), and modeling studies suggest that POC deposited tens of millions of years ago is still being slowly metabolized by microbial communi-

ties (Arndt et al., 2006; Røy et al., 2012; D'Hondt et al., 2015; LaRowe and Amend, 2015b; Bradley et al., 2018b, 2019). Since most sediment microorganisms depend on POC as an energy source, improved knowledge of the distribution and rates of POC degradation on a global scale is crucial to determining the extent, size and activity level of the vast deep biosphere. Intriguingly, the ability of microorganisms to process ancient POC calls into question some of the limits of life – i.e., how slowly can microorganisms metabolize, and over what time-scales can they remain viable.

The purpose of this communication is to simultaneously estimate the global distribution of marine sediment organic carbon, and the activity levels of microorganisms consuming it, throughout the Quaternary Period (0–2.59 Ma). By doing so, we improve understanding of the connection between short and long term carbon cycles, and the spatial distribution of microbial biomass in a large portion of the deep biosphere. The modeling approach builds on recent efforts to quantitatively describe marine sediments as a habitat for microbial life on a global scale (LaRowe et al., 2017). Several present-day global data sets, including bathymetry, sedimentation rates, POC concentrations at the sediment–water interface (SWI) and POC reactivity feed into these modeling efforts to provide maps of the distribution of organic carbon in global marine sediments. In addition, these data are used to constrain how much organic carbon resides and has been degraded in marine sediments deposited since the beginning of the Quaternary, which include the most microbially active portions of marine sediments. The resulting rates of organic carbon degradation and a bioenergetic power model are then combined to estimate the amount of power available to microorganisms in typical shelf, margin and abyssal sediments. Taken together, this global-scale quantitative description of carbon dynamics in marine sediments has implications for the long-term diagenesis of sediments and the bioenergetic limits of life.

2. METHODS

A 1-D reaction transport model, RTM, at a spatial resolution of $\frac{1}{4}^\circ \times \frac{1}{4}^\circ$ was used to calculate the amount of POC deposited, stored and degraded in marine sediments throughout the Quaternary. Due to dramatic differences in Earth's climate system between the Holocene (0 to 11,700 yrs ago) and Pleistocene (11,700 to 2.59 Myrs ago) Epochs, many of the parameterizations and therefore results shown below are given for these time periods. The Holocene sediment layers is further partitioned into bioturbated and non-bioturbated sections (see Fig. 1). The bioenergetic modeling carried out in this study uses the calculated rates of POC degradation to assess the activity levels and numbers of microorganisms in marine sediments.

Although most of the values of the parameters required to run the RTM are specified per grid cell, some of the model parameters are not well-constrained on a global basis (see Table 1). Consequently, we have selected values of these parameters that are characteristic of sediments found in three oceanic domains: shelf, margin and abyss (see

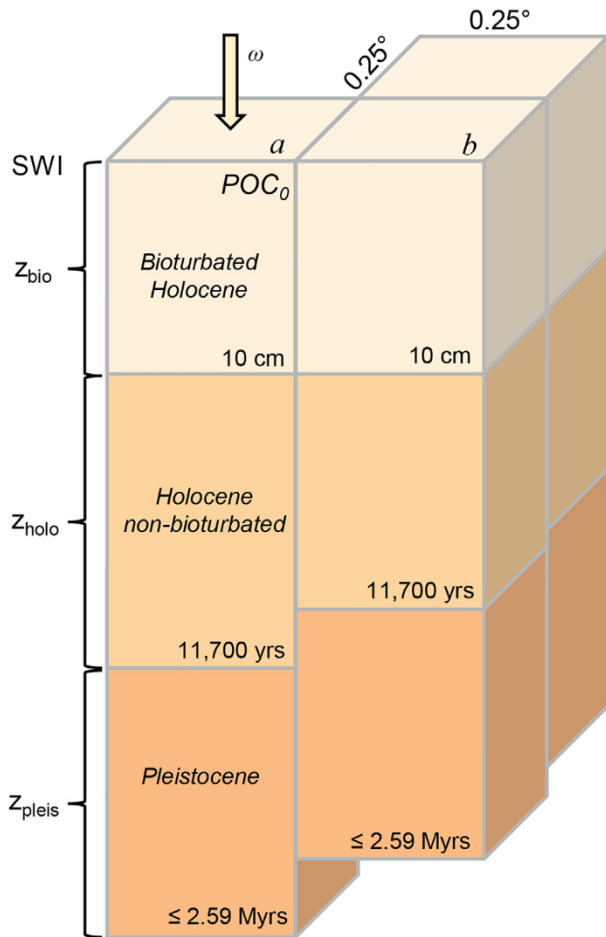


Fig. 1. Schematic structure of the model domain. For every grid cell in the model ($0.25^\circ \times 0.25^\circ$) there is a distinct sedimentation rate, ω , and concentration of particulate organic carbon at the sediment water interface (SWI), POC_0 . The bioturbated Holocene layer is 10 cm thick (i.e., z_{bio}) in every grid cell, except for locations where the Holocene sediment layer is less than 10 cm deep (see Fig. 3a). In these cases, the depth of the bioturbated zone was taken to be the maximum depth of the Holocene layer (i.e. for $z_{holo} < 10$ cm, $z_{bio} < 10$ cm). The thicknesses of the non-bioturbated Holocene (z_{holo}) and Pleistocene (z_{pleis}) layers are variable, depending on sedimentation rates, as indicated by the differing total depths of sediment columns *a* and *b*. Sediments at the bottom of the non-bioturbated Holocene layer are 11,700 years old. In some locations, sediments at the bottom of the Pleistocene layer are 2.59 Myrs old, the beginning of this Epoch. In locations where the ocean basement is not that old, or where seawater did not cover continental shelves during that Epoch, sediments at the bottom of the Pleistocene layer are less than 2.59 Myrs old (see Fig. 4).

Fig. 2). The location of each domain is defined by water depth (Vion and Menot, 2009): shelf environments roughly correspond to water depths < 200 m, with the exception of the Antarctic region where shelf area corresponds to water depths < 500 m; areas deeper than ~ 3500 m are taken to be abyssal plain; sediments under other water depths are referred to as margins. It follows that continental shelf underlies about 6.33% of ocean surface area, margins make up 10.78% and the abyssal domain constitutes the remaining 82.89%.

2.1. Reaction transport model

The one-dimensional conservation equation for POC in porous media is given by (e.g. Berner, 1980; Boudreau, 1997):

$$\frac{\partial(1-\phi)POC}{\partial t} = \frac{\partial}{\partial z} \left(D_b(1-\phi) \frac{\partial POC}{\partial z} \right) - \frac{\partial(1-\phi)\omega POC}{\partial z} + (1-\phi)R_{POC} \quad (1)$$

where POC corresponds to the concentration of particulate organic carbon (g C cm^{-3} dry sediment); t stands for time (yr); D_b refers to the bioturbation coefficient ($\text{cm}^2 \text{ yr}^{-1}$); ω represents the sedimentation rate (cm yr^{-1}) and R_{POC} denotes the rate of heterotrophic organic carbon degradation in units of g C cm^{-3} dry sediment yr^{-1} . The porosity, ϕ , of marine sediments in the shelf, margin and abyss domains was calculated as a function of depth, z (m) using a standard formulation commonly used in basin-to-global scale porosity studies (Athy, 1930) that assumes steady state compaction:

$$\phi(z) = \phi_0 \exp(-c_0 z) \quad (2)$$

where ϕ_0 denotes the porosity at the SWI and c_0 stands for the compaction length scale (m^{-1}), which characterizes how a given sediment type will compact under its own weight. The sources of all of values of the parameters appearing in Eqs. (1) and (2), as well as those in the following equation, are discussed in Section 2.3.

Quaternary sediments were divided into three layers which are mostly described as: bioturbated Holocene (top 10 cm (Boudreau, 1994; Solan et al., 2019)), non-bioturbated Holocene (10 cm to sediments $< 11,700$ yr) and Pleistocene (11,700 yr to 2.59 Myr). In the areas shown in Fig. 3a, the oldest Holocene sediments are less than 10 cm below the SWI. At these locations, the depth of the bioturbated zone matches the depth of Holocene sediments. Similarly, the map depicted in Fig. 3b shows where the sediments in contact with the basement are younger than the beginning of the Pleistocene. As a result, calculations covering these areas do not reach back 2.59 Myrs, but to the amount of time indicated in Fig. 3b. Sediment mixing was assumed to be constant over the bioturbated layer and non-existent immediately below it.

The rate of POC degradation, R_{POC} , was determined using a reactive continuum model, RCM. The RCM assumes a continuous, yet dynamic distribution of organic compounds comprising a range of reactivities and reproducing the often-observed decrease in apparent POC reactivity with depth, and thus burial age (Boudreau and Ruddick, 1991). Within the RCM, R_{POC} is given by:

$$R_{POC} = - \int_0^\infty k \cdot om(k, t) dk \quad (3)$$

where $om(k, t)$ denotes a probability density function that determines the concentration of organic carbon having a degradability between k and $k + dk$ at time t , with k (yr^{-1}) being analogous to a reaction rate constant. The initial distribution of organic compounds, $om(k, 0)$, may take

Table 1

Selected values of parameters used to characterize the porosity and organic carbon content of continental shelf, margin and abyss domains of global marine sediments.

Parameter	Definition	Shelf	Margin	Abyss	Units
ϕ_0	sediment porosity at the sediment-water interface ^a	0.45 ^a	0.74 ^{a,b}	0.7 ^a	(–)
c_0	sediment compaction length scale ^b	0.5×10^{-3a}	$1.7 \times 10^{-4a,b}$	0.85×10^{-3a}	m^{-1}
ia	reactive continuum age parameter				yr
	baseline	$10^{(3.35-14.81 \cdot \omega)c}$			
	low reactivity	5 ^d	3×10^{3e}	3.5×10^{4f}	
	high reactivity	3×10^{-4g}	3×10^{-4g}	20 ^h	
ν	reactive continuum distribution parameter				(–)
	baseline	0.125	0.125	0.125	
	low reactivity	0.135 ^d	0.16 ^e	0.16 ^f	
	high reactivity	0.125 ^g	0.125 ^g	0.16 ^h	

^a These values are representative of a sandstone-siltstone mixture (shelf), a sandstone-siltstone- shale combination (margin) and typical shales and biogenic-dominated sediments (abyss) (Hantschel and Kauerauf, 2009).

^b Wallmann et al. (2012).

^c Based on global compilation by Arndt et al. (2013), ω represents sedimentation rate, $cm\ yr^{-1}$.

^d Mogollón et al. (2012), Arkona Basin.

^e Wallmann et al. (2006), Sea of Okhotsk.

^f Middelburg (1989), Central Pacific.

^g Boudreau and Ruddick (1991) & Westrich and Berner (1984), fresh plankton material from Long Island Sound.

^h Marquardt et al. (2010), Peru.

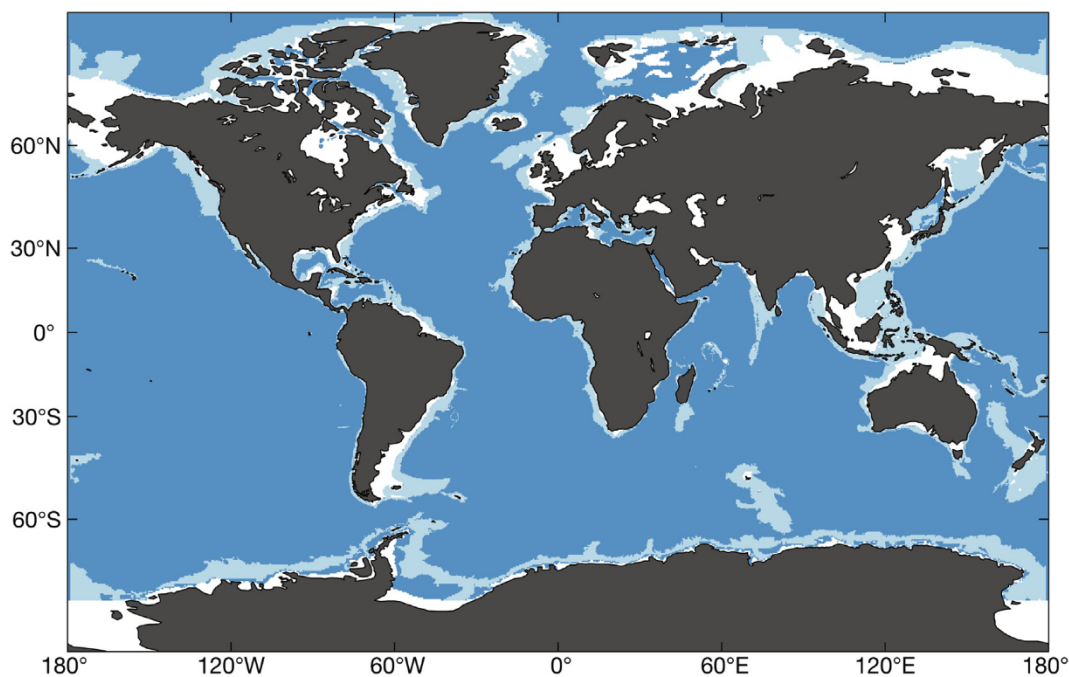


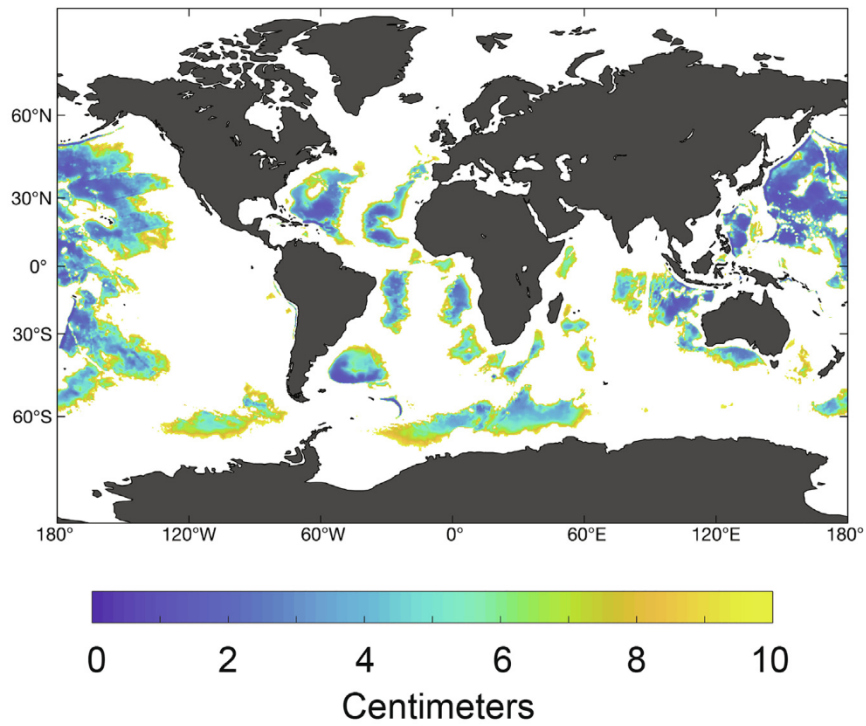
Fig. 2. Illustration of the shelf, margin and abyss domains considered in this study. The location of the continental margin boundaries was adopted from Vion and Menot (2009): shelf environments (white) roughly correspond to water depths <200 m, with the exception of the Antarctic region where shelf area corresponds to water depths <500 m; areas deeper than ~3500 m are taken to be abyssal plain (dark blue). The light blue regions correspond to the continental margin.

multiple mathematical forms, but cannot be inferred by observations. Here, a gamma function was used, as proposed by Boudreau and Ruddick (1991), following Aris (1968) and Ho and Aris (1987). Assuming first order degradation kinetics, the initial ($t = 0$) distribution of om over k is given by:

$$om(k, 0) = \frac{POC_0 \cdot ia^\nu \cdot k^{\nu-1} \cdot e^{-ia \cdot k}}{\Gamma(\nu)} \quad (4)$$

where POC_0 is the initial organic carbon content (at the SWI), Γ is the gamma function, ia (yr) is the average lifetime of the more reactive components of the mixture and

a)



b)

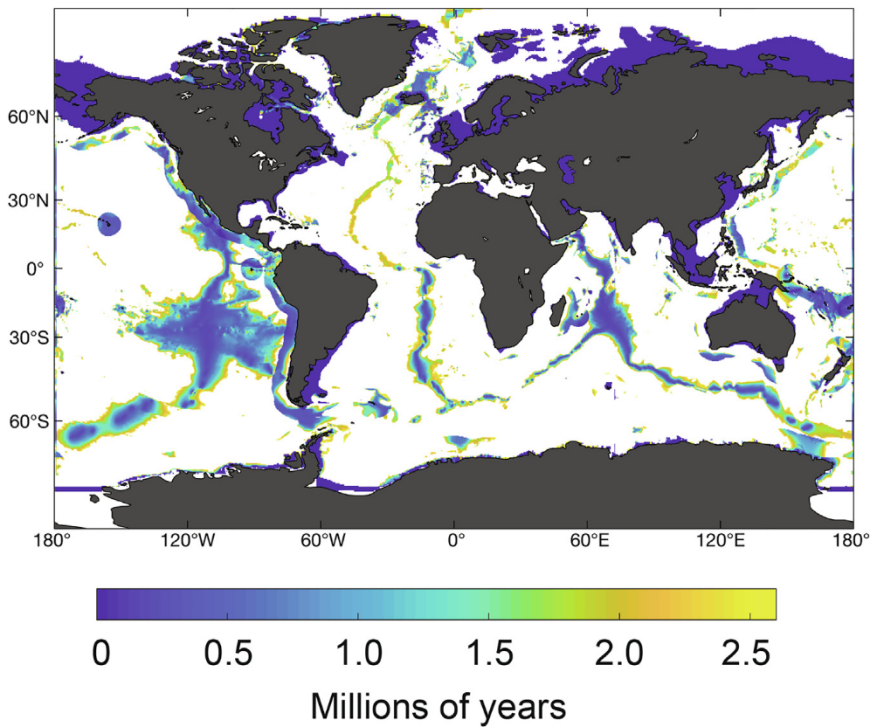


Fig. 3. (a) Areas where the oldest Holocene sediments are less than 10 cm below the sediment water interface (SWI); the indicated depths of these sediments coincide with the depth of the bioturbated Holocene layer. White areas correspond to locations where Holocene sediments are at least 10 cm deep. (b) Ages of sediment at the bottom of the Pleistocene sediment layer that are less than 2.59 million years. White areas indicate locations where sediments have been deposited at least since the beginning of the Pleistocene, whereas the other colors correspond parts of the ocean floor where the oldest Pleistocene sediments are younger than 2.59 Myrs.

v is a dimensionless parameter determining the shape of the distribution near $k = 0$. The adjustable, positive parameters ia and v completely determine the shape of the initial distribution of organic carbon compounds over the range of k values and thus the overall reactivity of POC. High v and low ia values indicate a mixture of organics dominated by compounds that are typically degraded rapidly. Low v and high ia values indicate a larger fraction of less reactive compounds that degrade slowly. See Arndt et al. (2013) for a more in-depth description of these parameters.

Although the choice of the gamma function is partly guided by mathematical expedience, it also has the advantage of describing the temporal evolution of organic carbon profiles observed in sediments. Assuming steady state conditions ($\frac{\partial POC}{\partial t} = 0$) and a known organic carbon content at the sediment water interface, POC_0 , the change in the bulk particulate organic carbon concentration as a function of depth, $POC(z)$, is given by Boudreau and Ruddick (1991):

$$POC(z) = POC_0 \cdot \left(\frac{ia}{ia + age(z)} \right)^v \quad (5)$$

where $age(z)$ refers to the age of the sediment layer at depth z . While the RCM has proven successful in predicting the down-core evolution of organic carbon reactivity in deep sediments, its application to the bioturbated layer of sediment is compromised by the difficulty of constraining the age of organic carbon in bioturbated sediments. Meile and Van Cappellen (2005) showed that, within the bioturbated zone, the age distribution of reactive species is not only controlled by bioturbation and sedimentation but also by the reactivity of the species in question. Similar to the approach proposed by Dale et al. (2015) and Dale et al. (2016), we use a multi-G approximation of the RCM for bioturbated sediments because the age of POC in them cannot be well-constrained (see Appendix A).

Below the bioturbated Holocene zone, the values of $age(z)$ that are required to evaluate Eq. (5) were calculated using sediment burial rates, $\omega(z)$, porosity depth profiles, $\phi(z)$, and the apparent age of organic carbon at the lower limit of the bioturbated Holocene zone, $age_{z_{bio}}$. The latter was calculated by inserting POC_{bio} and $age_{z_{bio}}$ into Eq. (5) for $POC(z)$ and $age(z)$, respectively, and solving for the age:

$$age_{z_{bio}} = \frac{-ia \cdot (\exp(\ln(POC_{bio}/POC_0)/v) - 1)}{\exp(\ln(POC_{bio}/POC_0)/v)} \quad (6)$$

Assuming an exponentially decreasing porosity, Eq. (2), and steady-state compaction, the sediment burial velocity, ω , at depth z is then (e.g. Berner, 1980):

$$\omega(z) = \left(\frac{1 - \phi_0}{1 - \phi(z)} \right) \omega_0 \quad (7)$$

where ω_0 corresponds to the sediment burial velocity at the SWI. The age of a given sediment layer at depth z below the bioturbated Holocene zone, $age(z)$, is given by

$$age(z) = \int_0^z \omega^{-1} dz \quad (8)$$

Substituting Eq. (7) into Eq. (8) results in

$$age(z) = \frac{1}{(1 - \phi_\infty)\omega_\infty} \int_0^z (1 - \phi) dz \quad (9)$$

which, upon integration, leads to

$$age(z) = \frac{z + \frac{\phi_0}{c_0} \cdot (\exp(-c_0 \cdot z) - 1)}{\omega_0 \cdot (1 - \phi_0)} \quad (10)$$

The age of POC below the bioturbated Holocene zone is thus given by:

$$age(z) = age_{z_{bio}} + \frac{z + \frac{\phi_0}{c_0} \cdot (\exp(-c_0 \cdot (z - z_{bio})) - 1)}{\omega_0 \cdot (1 - \phi_0)} \quad (11)$$

The depth distribution of organic carbon in marine sediments deposited since the beginning of the Quaternary can thus be calculated with knowledge of the sedimentation rate, level of bioturbation, porosity structure, bulk organic carbon concentration at the SWI and the distribution of organic compounds across the reactivity range at the SWI.

2.2. Total POC budget and burial efficiency

The total amount of POC stored in the i th sediment layer ($i =$ bioturbated Holocene (0 to z_{bio}), non-bioturbated Holocene (z_{bio} to z_{holo}), Pleistocene (z_{holo} to z_{pleis})), $\bar{P}OC_i$ (g C cm⁻²), is given by:

$$\bar{P}OC_i = \int_{z_i}^{z_{i-1}} POC(z) dz \quad (12)$$

where the z_{i-1} and z_i refer to the upper and lower boundaries, respectively, of the sediment horizon of interest.

The amount of POC degraded in the non-bioturbated layer i , \bar{R}_i , is given by

$$\bar{R}_i = \int_{z_i}^{z_{i-1}} k(z) \cdot POC(z) dz \quad (13)$$

The depth-integrated amount of POC degraded in the bioturbated Holocene layer, $\bar{R}_{z_{bio}}$, is calculated as the difference between the deposition flux, F_{dep} , and the burial flux through the depth of the bioturbated layer, $F_{z_{bio}}$ (see Eqs. (16) and (17)), and thus also accounts for the amount of POC degraded during incorporation into the sediment (i.e. at the sediment water interface):

$$\bar{R}_{z_{bio}} = F_{dep} - F_{z_{bio}} \quad (14)$$

Carbon burial efficiencies, BE (%), which reveal the proportion of POC that has survived microbial degradation to a given sediment horizon, have also been calculated. Values of BE are therefore a concise way of combining all the forces in an ecosystem that work to degrade and protect organic carbon. The way that burial efficiencies are calculated here reveals how much of the steady state flux of POC that has been deposited at the sediment water interface for each sediment layer is buried through a particular sediment horizon defined by its age (i.e., z_{bio} , z_{holo} , z_{pleis}). This is in contrast to how BE is typically calculated, as a flux of POC through a particular sediment depth, which ignores differing sedimentation rates and thus the differing amounts of time that POC has been degraded.

Here, BE is taken to be the amount of POC that has fluxed through a given sediment age, which corresponds to different depths (see Figs. 3 and 4), F_z ($\text{g C cm}^{-2} \text{ yr}^{-1}$), relative to the steady state depositional flux through the sediment water interface of the respective depth layers/time periods, F_{dep} ($\text{g C cm}^{-2} \text{ yr}^{-1}$):

$$BE = F_z / F_{dep} \tag{15}$$

where

$$F_z = (1 - \phi(z))D_b \left. \frac{dPOC(z)}{dz} \right|_z + (1 - \phi(z))\omega \cdot POC(z) \tag{16}$$

Note that for sediment depth $z \geq z_{bio}$, transport becomes purely advective and the dispersion term in Eq. (16) is dropped. Values of F_{dep} were calculated using

$$F_{dep} = (1 - \phi(0))D_b \left. \frac{dPOC(0)}{dz} \right|_0 + (1 - \phi(0))\omega \cdot POC(0) \tag{17}$$

Note that $\left. \frac{dPOC(0)}{dz} \right|_0$ is determined by the first derivative of Eq. (A.9), the analytical solution to Eq. (1), and thus varies with POC reactivity (i.e. parameters ia and v), the bioturbation coefficient and sedimentation rate. Also note that two

different sets of values for ω , the sedimentation rate, are used: one for Holocene sediments and the other for Pleistocene sediments (see below).

2.3. Parameters and forcings

As described below, each grid cell has particular values of POC_0 , ω_0 , D_b , ia (for the baseline scenario) and z , whereas values of ϕ_0 , v , ia (for the low and high-reactivity scenarios) and c_0 are assigned to grid cells depending on whether their water depth places them in the shelf, margin or abyss domains (see Fig. 2 and Table 1).

The concentration of POC at the sediment water interface, POC_0 , for Holocene sediments was taken from a global compilation of these values (Seiter et al., 2004; Romankevich et al., 2009) (see Wallmann et al., 2012). Holocene sedimentation rates, ω , were calculated using an algorithm that correlates water depth and sedimentation rate according to a double logistic equation (Burwitz et al., 2011), building on Holocene sedimentation data from over 500 stations (Betts and Holland, 1991; Colman and Holland, 2000; Seiter et al., 2004). The total global sedimentation rate for the Pleistocene was taken to be the same as that for the Holocene, but the spatial distribution of

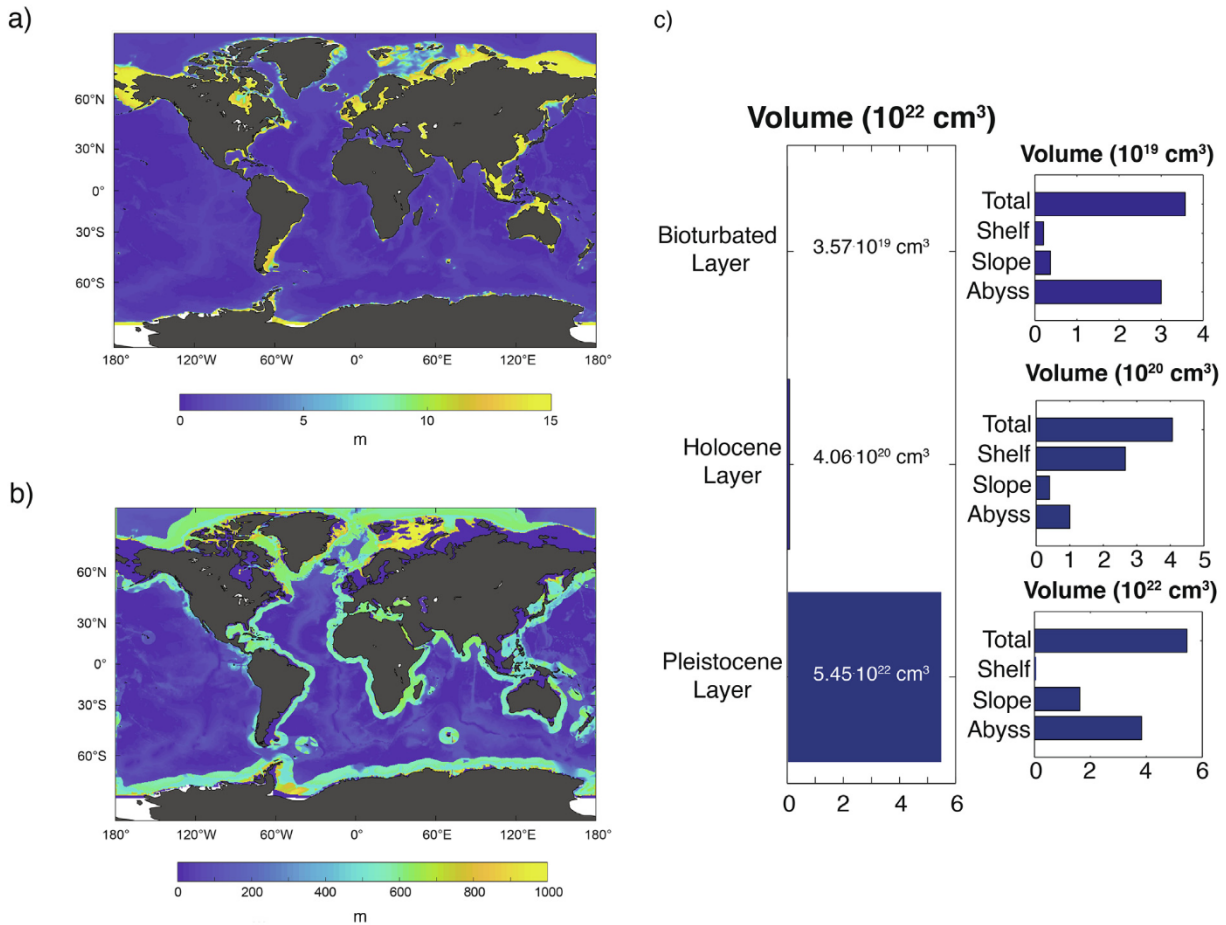


Fig. 4. Maximum depths to which (a) Holocene and (b) Pleistocene sediments reach (note different scales). (c) Total volumes of bioturbated Holocene, non-bioturbated Holocene and Pleistocene sediments and how these volumes are partitioned among the shelf, margin and abyss domains.

where this sedimentation occurred was changed to take into account lower sea level (Menard and Smith, 1966; Peltier, 1994; Rohling et al., 1998; Ludwig et al., 1999), altered patterns of dust deposition and the transport of ice-rafted material (Lisitzin, 1996) during this Epoch. Consequently, sedimentation rates on margins were increased by a factor of five over a 500 km wide zone around continental margins (Burwicz et al., 2011), while sedimentation velocities on shelves were decreased such that global sedimentation during the Pleistocene matched that of the Holocene. The resulting Pleistocene sedimentation rates were used with the distribution of Holocene POC to calculate the distribution of Pleistocene POC concentrations at the SWI (see Wallmann et al., 2012). It should be noted that this partitioning of Holocene vs Pleistocene sedimentation rates might not exactly reproduce regional sedimentation histories everywhere, e.g. in the North Sea (Lamb et al., 2018), but this method has been chosen to account for global patterns of sedimentation during the Quaternary (see below).

The bioturbation coefficient, D_b , was calculated as a function of water depth based on a compilation of empirical data (Middelburg et al., 1997). Its values range from 27 to $0.59 \text{ cm}^2 \text{ yr}^{-1}$, decreasing in magnitude as water depth increases. It is constant throughout the bioturbated Holocene zone and immediately drops to zero beneath it.

For simplicity and clarity, values of porosity at the sediment water interface, ϕ_0 , and the compaction length scale, c_0 , were chosen to describe the shelf, margin and abyss based on sediments that are representative of these domains (Hantschel and Kauerauf, 2009) (see Table 1).

The reactivity of organic carbon deposited onto the seafloor and its evolution during burial is notoriously difficult to constrain. In general, the organic carbon reactivity parameters of the 1G-model, k , and the RCM, ia and v , are determined by finding a best fit to observed POC and pore-water profiles at specific sites (e.g. Arndt et al., 2013). However, because heterotrophic degradation of organic carbon involves a plethora of different organisms that breakdown a wide range of organic compounds under varying environmental conditions, using a number of different terminal electron acceptors and producing a large range of different product compounds (see LaRowe et al., 2020), attempts to identify statistically significant relationships between organic carbon degradation rate constants and individual factors such as water depth, deposition rate, or organic carbon flux on a global scale have not been definitively established. Stolpovsky and colleagues have proposed empirical relationships among benthic O_2 and NO_3^- fluxes to estimate parameter values for POC degradation models that employ power-law and multi-G functions (Stolpovsky et al., 2015, 2018), but there is currently no general framework that can be used to estimate the ia and v parameters in the RCM on a global scale. Consequently, organic carbon reactivities are associated with large uncertainties.

Here, we considered three levels of organic carbon reactivity for each domain: a baseline scenario as well as minimum and maximum reactivity parameter sets based on the lower and upper bounds of published values, henceforth

referred to as the low- and high-reactivity scenarios (see Table 1). The baseline scenario is constrained not only by a global parameter compilation, but also on observations that the v parameter values do not vary much between sites, while the ia parameter can vary over orders of magnitude (e.g. Boudreau and Ruddick, 1991; Arndt et al., 2013). Therefore, for the baseline scenario we chose a constant v parameter of 0.125, characteristic of fresh organic carbon (Boudreau et al., 2008). Values of the ia parameter are correlated with sedimentation rates based on a global compilation of RCM applications (Arndt et al., 2013). This approach accounts for order-of-magnitude changes in ia due to factors that control OM transit times from its source to deposition. The baseline scenario thus reflects typically observed RCM parameter variability across various depositional environments, while the parameters chosen for the high and low reactivity scenarios span nearly the entire range of observed values reported in the literature (e.g. Boudreau and Ruddick, 1991; Arndt et al., 2013).

Several processes that could impact global rates of POC degradation have not been included in the model presented above, and some of the formulations used could be improved in future studies. For instance, our model does not take into account the production of POC in sediments by phototrophs in shallow waters (Middelburg, 2018, 2019) and, globally, by chemoautotrophy (Veuger et al., 2012; Sweetman et al., 2017), a process that has been estimated to contribute as much as $0.29 \text{ Pg C yr}^{-1}$ to near-shore and shelf sediments (Middelburg, 2011). In addition, it is unlikely that our model captures the heterogeneity, dynamic nature, transient conditions and other complex factors that characterize POC in sediments underlying portions of the coastal ocean. Also, the simple re-partitioning of Holocene sedimentation patterns from the shelf domain to towards deeper waters for Pleistocene sedimentation rates is a simplification that could be scaled to paleobathymetry, similar to other parameters considered in this study. Finally, post-depositional erosion or transport of sediment is not explicitly included as impacting POC reactivity. However, because a large compilation of POC concentrations in the top 5 cm of sediment has been used (Seiter et al., 2004), this could partly be taken into account.

2.4. Bioenergetics calculations

We have taken the approach used by LaRowe and Amend (2015a, 2015b) to relate the rates and energetics of organic carbon degradation to the number of microbial cells that an environment can support. Briefly, the amount of biomass, B (cells cm^{-3}), that can be sustained by a given amount of energy per unit time, (or power) is calculated with

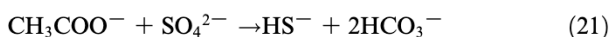
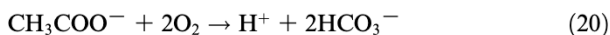
$$B = \frac{P_s}{P_d} \quad (18)$$

where P_s (W cm^{-3}) and P_d (W cell^{-1}) denote the volumetric power supply and the cellular power demand, respectively. Values of P_s are calculated using

$$P_s = \Delta G_r \cdot R_{POC} \quad (19)$$

where values of R_{POC} are calculated using Eq. (3) and ΔG_r is computed as described below. The values of P_d used for organisms oxidizing POC with oxygen and sulfate are the median values of those collected by LaRowe and Amend (2015a): for aerobic heterotrophy it is 2375 fW cell⁻¹ and for sulfate reduction it is 77 fW cell⁻¹.

The amount of energy available from the oxidation of organic carbon by aerobic and sulfate-reducing pathways, which are assumed to be the two main pathways of POC degradation in marine sediments (Archer et al., 2002; Canfield et al., 2005; Jørgensen and Kasten, 2006; Thullner et al., 2009), were calculated using acetate as a proxy for organic carbon (see below):



and the Gibbs energy function,

$$\Delta G_r = \Delta G_r^0 + RT \ln Q_r \quad (22)$$

where ΔG_r^0 and Q_r refer to the standard molal Gibbs energy and the reaction quotient of the indicated reaction, respectively, R represents the gas constant, and T denotes temperature in Kelvin. Values of ΔG_r^0 were calculated using the revised-HKF equations of state (Helgeson et al., 1981; Tanger and Helgeson, 1988; Shock et al., 1992), the SUPCRT92 software package (Johnson et al., 1992), and thermodynamic data taken from a number of sources (Shock and Helgeson, 1988; Shock et al., 1989; Shock and Helgeson, 1990; Sverjensky et al., 1997; Schulte et al., 2001). Values of Q_r are calculated using

$$Q_r = \prod_i a_i^{v_i} \quad (23)$$

where a_i stands for the activity of the i th species and v_i corresponds to the stoichiometric coefficient of the i th species in the reaction of interest (e.g. Rxns. (20) and (21)). Molalities of the i th species, m_i , were converted into activities using individual activity coefficients of the i th species (γ_i),

$$a_i = m_i \gamma_i. \quad (24)$$

Values of γ_i were in turn computed as a function of temperature and ionic strength using an extended version of the Debye-Hückel equation (Helgeson, 1969).

Temperatures and pressures in marine sediments vary considerably (LaRowe et al., 2017), as do concentrations of the reactants and products in Reactions (20) and (21). Hence, it is impossible to calculate single, globally relevant values of the Gibbs energies of organic carbon oxidation by O_2 and SO_4^{2-} . However, to facilitate the bioenergetic analysis presented below, we have selected two sets of conditions for calculations of ΔG_r . For shelf and margin sediments, we used $\Delta G_r = -81.5 \text{ kJ (mol acetate)}^{-1}$ (Rxn (20), $\log a_i$ for acetate, SO_4^{2-} , HS^- and HCO_3^- were taken to be -3.2 , -2.6 , -7.2 and -2.9 at 5 °C and 100 bars of pressure), while for abyss sediments, $\Delta G_r = -841.6 \text{ kJ (mol acetate)}^{-1}$ (Rxn (21), $\log a_i$ for acetate, O_2 and HCO_3^- taken to be -3.2 , -3.5 and -2.9 , pH = 8 at 5 °C and 400 bars of pressure; see Amend and LaRowe, 2019) for relevant values of activity coefficients). These assumptions

effectively assume that POC is degraded by sulfate reducing organisms in shelf and margin settings and by aerobic metabolism in abyssal sediments (see Jørgensen and Kasten (2006) and D'Hondt et al. (2015)). Although other oxidants are used by microorganisms for degrading organic carbon in marine sediments, such as nitrate and Fe-oxides, as well as breakdown by fermenters, only O_2 - and SO_4^{2-} -mediated POC degradation are considered here because the vast majority of marine sedimentary organic carbon is thought to be degraded via these pathways (Canfield et al., 2005; Jørgensen and Kasten, 2006; Thullner et al., 2009). Acetate is used as a proxy for organic carbon in Reactions (20) and (21) since there are thousands of organic compounds that microorganisms could be oxidizing and the identities (and likely, the thermodynamic properties) of the organic molecules consumed by microorganisms in natural settings is rarely known. In addition, the Gibbs energies of OM degradation are, on a per electron basis, much more sensitive to the identity of the electron acceptor than that of the organic compound (LaRowe and Van Cappellen, 2011; LaRowe and Amend, 2015a), so by focusing on the oxidant, we are capturing the first-order energetic differences of OC degradation in different environmental settings. Finally, it is worth noting that as a common fermentation byproduct, acetate is a regular constituent of marine sediment pore water (Glombitza et al., 2015 and references therein).

3. RESULTS

The reaction transport model described above has been used to assess the fate of POC in shelf, margin and abyss sediments according to three POC reactivity scenarios for sediments deposited throughout the Quaternary. The results are presented for the bioturbated Holocene (top 10 cm except where $z_{Holo} < 10 \text{ cm}$, see Fig. 3a), non-bioturbated Holocene (from 10 cm to sediments that are 11,700 yrs old, where $z_{holo} > 10 \text{ cm}$) and Pleistocene (from 11,700 to 2.59 Myrs for locations where sediments reach this age; see Fig. 3b) sediment layers (see Fig. 2). The rates of POC degradation in typical shelf, margin and abyss domains are also used to illustrate the power levels sustaining microbial communities in these environments as a function of depth. The model calculates steady state POC in the indicated temporal sediment layers. For conceptual clarity, all organic carbon beneath the bioturbated zone goes from the SWI, through a bioturbated zone and then out of it into the respective sediment horizons, the non-bioturbated Holocene, and for older sediments, into the Pleistocene layer.

3.1. Structure of sediment layers

Due to spatially heterogeneous sedimentation rates (Wallmann et al., 2012), the thickness of Holocene and Pleistocene sedimentary layers varies considerably as a function of longitude and latitude. In Fig. 4a, it can be seen that Holocene sediments can extend to about 15 m below the SWI (yellow colors) in many coastal locations, particularly in high northern latitudes, the eastern side of South America, between Southeast Asia and Indonesia, the East

China Sea and the Arafura Sea. Most of the rest of the ocean's Holocene sediments are <1 m thick (dark blue colors in Fig. 4a). The thickness of Pleistocene sediments, shown in Fig. 4b, also displays the impact of differential sedimentation rates. Using a different scale, Pleistocene sediments are shown to be up to 1000 m thick, mostly in high latitudes. Looking like a teal halo, there is a considerable proportion of Pleistocene sediments between ~500–700 m thick surrounding most land-masses. As is also illustrated in Fig. 3b, the areas close to land where there are little to no Pleistocene sediments, colored dark blue, were largely not covered by seawater during this Epoch (Hay, 1994).

The volumes of the bioturbated Holocene, non-bioturbated Holocene and Pleistocene sediment layers, as well as their relative distributions in the shelf, margin and abyss domains are shown in Fig. 4c. These values are given in units of cm^3 because microbial biomass concentrations are often reported in units of cells cm^{-3} . The, mostly, 10 cm-thick bioturbated Holocene layer has a total volume of $3.6 \times 10^{19} \text{ cm}^3$, containing $1.1\text{--}1.7 \times 10^{17} \text{ g}$ of organic carbon (Table 3); the vast majority of this layer is located in the abyss domain. The non-bioturbated Holocene layer, by comparison, is an order of magnitude more voluminous, at $\sim 4.1 \times 10^{20} \text{ cm}^3$, with $7.1\text{--}25 \times 10^{17} \text{ g}$ organic C (Table 3). Most of the Pleistocene sediments, contrary to the non-bioturbated Holocene layer, are in the abyss domain with a minuscule proportion on shelves (Fig. 4c). Interestingly, even though the Pleistocene lasted ~220 times longer than the Holocene, Pleistocene-aged sediments only occupy about 100 times the volume of non-bioturbated Holocene sediments. This is partly attributable to lower sedimentation rates and lower sea levels before the Holocene and the compaction of sediments that has taken place at depth.

3.2. Burial efficiency

The percentage of POC that has been buried through the bioturbated Holocene, non-bioturbated Holocene, and Pleistocene sediment layers relative to the amount that fluxed through the SWI is shown in Fig. 5 and Table 2 for the three POC reactivity scenarios considered in this study. The spatial distribution of BEs in all three reactivity scenarios is heterogeneous, though less so in the high reactivity case. Because all of the plots are presented on the same scale, the variability in BE for the high-reactivity case is best seen in Table 2. Fig. 5g–i and Table 2 show that almost no (<0.1%) POC arriving at the SWI is buried beneath the three sediment layers and three domains considered here, except for abyssal sediments where values of BE are slightly higher (~2%). By contrast, values of BE for abyssal sediments in the low reactivity scenario range from 50% to 66% for the three sediment layers. However, global BEs for the low-reactivity scenario are less than ~8% in both of the Holocene layers. BE in the baseline scenario range from 20% through the bioturbated Holocene layer to about 12% through the non-bioturbated Holocene and 24% through the Pleistocene layers.

3.3. POC budget for each time interval

The masses of POC stored in the bioturbated Holocene, non-bioturbated Holocene and Pleistocene sediment layers for the shelf, margin and abyss domains are given in Table 3 for all three reactivity scenarios. The different scenarios show similar amounts of POC retained in the baseline and low-reactivity cases, but considerably lower amounts in the high-reactivity scenario for shelf and margin sediments. It can also be seen that for each reactivity scenario, there are patterns to which sediment type (shelf, margin, abyss) contains the least and most amount of POC: for bioturbated Holocene sediments, the most POC resides in abyss settings and the least in margin sediments. Similarly, for non-bioturbated sediments the least POC is in margin settings, but the most is in shelf environments. Finally, the amount of POC stored in the Pleistocene layer follows water depth – the most POC is stored in the abyss for all three reactivity scenarios and the least in the shelf.

The integrated amounts of POC stored in each sediment layer for the baseline scenario are shown in the maps displayed in Fig. 6. The distribution patterns of POC in the top two layers is nearly uniform (Fig. 6a), with some outliers in near-coastal regions for the non-bioturbated sediments (green colors in Fig. 6b). Not surprisingly, orders of magnitude more POC is stored in the much larger volume of Pleistocene sediments (Fig. 6c).

3.4. Microbial rates of POC degradation

The overall rates of POC degradation in the three sediment layers are shown in Table 4 for each of the three reactivity scenarios. Illustrating the importance of the ia and v RCM parameters on the most recently deposited sediments, the rates of POC degradation are orders of magnitude higher in the high reactivity scenario in bioturbated Holocene sediments than in the other two cases. However, global rates are lower in the non-bioturbated Holocene and Pleistocene sediments for the high reactivity scenario than for the baseline and low reactivity scenarios, which are nearly the same.

The integrated rates of POC degradation by microorganisms in the different sediment horizons are shown in Fig. 7 for the baseline scenario. For each layer, the rates vary by orders of magnitude depending on, mostly, distance from land. The rates tend to be highest in shelf and margin sediment layers, with abyssal rates up to several orders of magnitude lower.

The rates of POC degradation at the bottoms of the non-bioturbated Holocene and Pleistocene sediment layers are shown in Fig. 8 for the baseline reactivity scenario. As in the amounts of POC stored and the integrated rates of POC degradation, there are strong geographical differences in rates at the oldest sediments for each layer. POC degradation rates at the bottom of Holocene typically fall between 10^{-9} and $10^{-7} \text{ g C cm}^{-3} \text{ yr}^{-1}$ (Fig. 8a), while those at the bottom of the Pleistocene tend to be two orders of magnitude slower; the sediments near land in high northern latitudes are one exception, however (Fig. 8b).

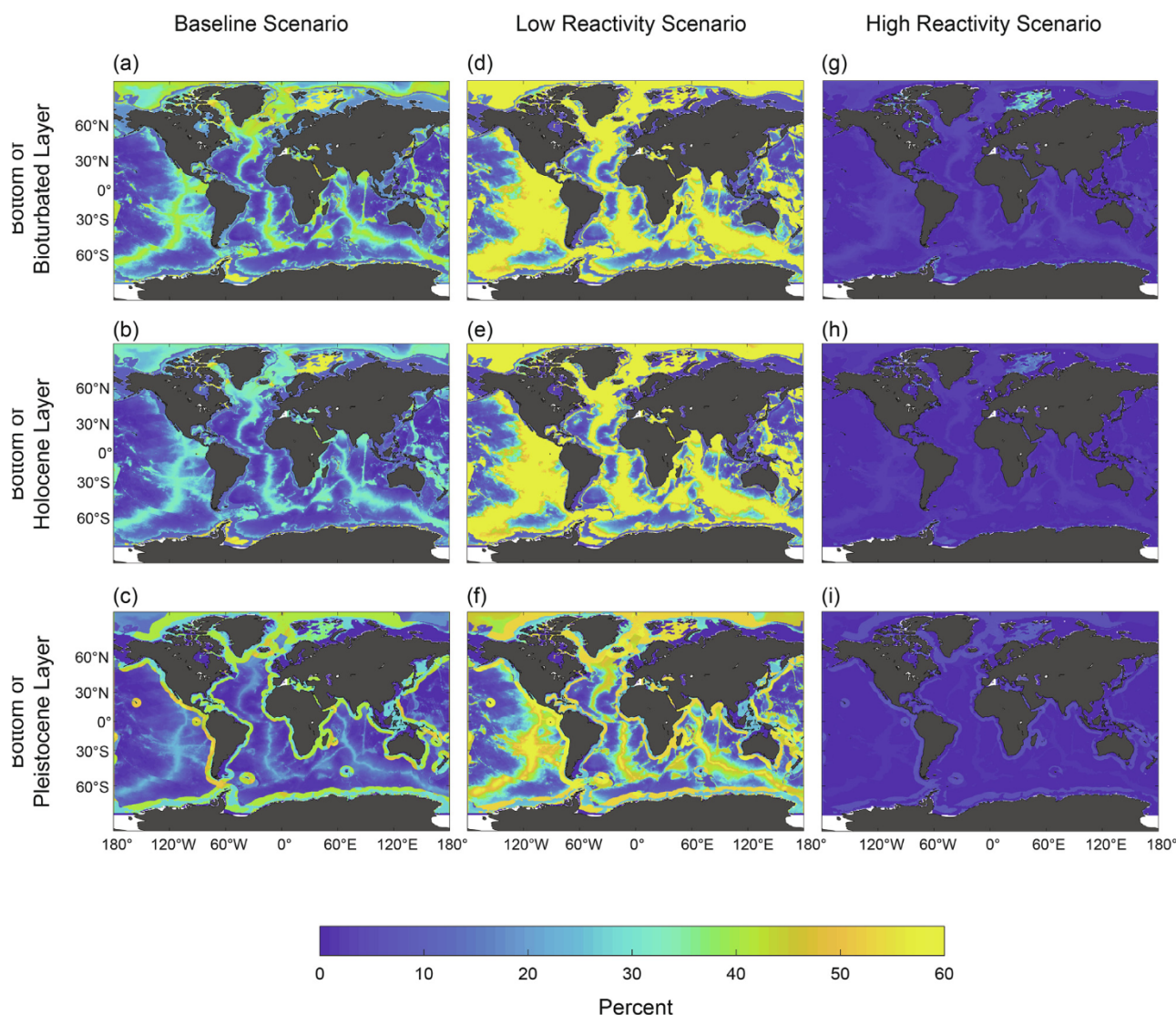


Fig. 5. Burial efficiencies, BE , of particulate organic carbon, POC, through the bioturbated Holocene (a, d, g) non-bioturbated Holocene (b, e, h) and Pleistocene (c, f, i) sediment layers for the baseline (a–c), low (d–f) and high (g–i) POC reactivity scenarios considered in this study. The values of BE are given as the percent of POC that has fluxed through a given sediment *age* relative to the depositional flux through the sediment water interface (see Eqs. (15)–(17)).

3.5. POC power

The amount of power available to microorganisms due to the oxidation of POC in representative shelf, margin and abyss sediments is shown as a function of sediment depth in Fig. 9a. For all three domains, the power available from POC degradation spans several orders of magnitude from the SWI to sediments that were deposited at the beginning of the Pleistocene. The somewhat complex shapes of these curves are due to the different algorithms used to calculate POC degradation in the bioturbated Holocene layer and the rest of the sediment column. Despite their apparent separation on this log-log plot, the power supply in margin and abyss sediments is nearly the same, starting at $10^{-11} \text{ W cm}^{-3}$ and dropping to $\sim 4 \times 10^{-15} \text{ W cm}^{-3}$. Values of P_s in the shelf setting start two orders of magnitude higher than

the other locations and decrease to about $10^{-14} \text{ W cm}^{-3}$ at the bottom of the Pleistocene. The calculated power supply and biomass content in sediments do not follow the same trend in abyss and margin sediments because we have assumed that most microbial power in the abyss is from aerobic respiration and in margin sediments from sulfate reduction. According to the laboratory-based literature (LaRowe and Amend, 2015a), the maintenance powers for these classes of organisms are significantly different (see Methods section), so power and biomass in these realms do not follow the same proportionality.

In order to produce global-scale estimates of biomass density, one would need to know which reaction is being catalyzed for energy and its corresponding value of ΔG_r . This requires data such as pore water composition that are not globally available. However, the representative

Table 2

Flux of particulate organic carbon (POC) through the sediment water interface (SWI), bioturbated Holocene, non-bioturbated Holocene and Pleistocene sediment layers in the baseline and low and high POC reactivity scenarios considered in this study. Note that the flux of POC through the SWI for the Pleistocene is different than the Holocene. Burial efficiencies (*BE*), calculated as shown in Eq. (15), are also given.

Reactivity scenario:	Baseline		Low		High	
flux units are 10^{13} g C yr ⁻¹	flux	<i>BE</i> (%)	flux	<i>BE</i> (%)	flux	<i>BE</i> (%)
SWI (Bioturb. & Holocene)						
Shelf	138	–	383	–	27,900	–
Margin	10.2	–	8.54	–	11,500	–
Abyss	16.0	–	6.67	–	105	–
Total	164.2	–	398	–	39,505	–
Bioturbated Holocene layer						
Shelf	26.8	19.4	22.8	6.0	7.24	0.026
Margin	1.85	18.1	1.86	21.8	0.40	0.004
Abyss	4.16	26.0	4.42	66.3	2.56	2.44
Total	32.8	20.0	29.1	7.3	10.2	0.03
Non-bioturbated Holocene layer						
Shelf	14.5	10.5	10.2	2.7	3.27	0.012
Margin	1.40	13.7	1.48	17.3	0.21	0.002
Abyss	3.41	21.3	4.27	64.0	1.61	1.53
Total	19.4	11.8	15.9	4.0	5.09	0.01
SWI (Pleistocene)						
Shelf	2.57	–	4.23	–	27,900	–
Margin	12.6	–	11.3	–	11,500	–
Abyss	24.8	–	17.4	–	110	–
Total	40.0	–	32.9	–	39,510	–
Pleistocene layer						
Shelf	0.0077	0.3	0.0049	0.1	2.63	0.009
Margin	2.96	23.5	2.58	22.8	0.43	0.004
Abyss	6.78	27.3	8.63	49.6	2.63	2.39
Total	9.75	24.4	11.2	34.0	5.69	0.01

The depth of the bioturbated layer is set to 10 cm, but the depths of the Holocene and Pleistocene layers are based on their ages and are therefore variable (see Fig. 4). For locations where the Holocene sediment layer is less than 10 cm deep (see Fig. 3a), the depth of the bioturbated zone was taken to be the maximum depth of the Holocene layer (i.e. for $z_{\text{holo}} < 10$ cm, $z_{\text{bio}} < 10$ cm).

power densities shown in Fig. 9a can be compared to published and collated maintenance powers, P_d , of microorganisms carrying out aerobic and sulfate-consuming heterotrophy (LaRowe and Amend, 2015a) to estimate how many microorganisms are simply carrying out maintenance functions in marine sediments (if growth is accounted for, additional model parameters would be needed, e.g. LaRowe and Amend (2016); Bradley et al. (2018a)). The amount of biomass that could be supported on maintenance power alone for the three representative sediment columns shown in Fig. 9a are shown in Fig. 9b. The number of cells at the SWI for representative shelf, margin and abyss sediments are 4×10^4 , 280 and 5 cell cm^{-3} , dropping to less than 1 cell cm^{-3} for sediments that were deposited at the beginning of the Pleistocene.

4. DISCUSSION

There are published estimates of the global flux of organic carbon to marine sediments, the amount degraded in surface sediments and the quantity buried (see below). However, there are no 3-D maps revealing quantitative estimates of the physical distribution of these fluxes, the

amounts of organic carbon expected to be found at particular depths and locations, and therefore, additionally, the metabolic rates of microorganism in the deep biosphere on a global scale. Furthermore, our estimates are based on the age of sediment horizons, not simply their depths. The results presented in this study demonstrate not only where organic carbon is likely distributed in marine sediments in three dimensions, but how much has been degraded by microbial activity and how much remains in particular horizons over the last ~2.6 million years in three dimensions. This information is useful for understanding the long-term carbon cycle, the extent of the marine sedimentary biosphere and the location and vigor of diagenesis. The specific implications of the results of this study are presented below.

4.1. Quaternary organic carbon budget

An understanding of organic carbon preservation and burial in marine sediments is critical to interpret the sedimentary isotope record and quantify carbon sources and sinks over geological time scales (Bernier, 2004). Here, we reveal the most comprehensive, spatially-resolved quantita-

Table 3

Storage of particulate organic carbon, POC, in the bioturbated Holocene, non-bioturbated Holocene and Pleistocene layers in the baseline and low and high POC reactivity scenarios considered in this study.

Units are 10^{17} g C	Baseline	Low reactivity	High reactivity
Bioturbated Holocene layer			
Shelf	0.250	0.231	0.096
Margin	0.196	0.196	0.063
Abyss	1.23	1.27	0.946
Total	1.68	1.70	1.11
Non-bioturbated Holocene layer			
Shelf	19.1	13.5	4.29
Margin	1.74	1.83	0.269
Abyss	4.08	5.00	2.52
Total	24.9	20.4	7.08
Pleistocene layer			
Shelf	1.09	0.708	0.234
Margin	428	466	62.2
Abyss	1000	1440	403
Total	1429	1907	465

The depth of the bioturbated layer is fixed at 10 cm, but the depths of the Holocene and Pleistocene layers are based on their ages and are therefore variable (see Fig. 4). For locations where the Holocene sediment layer is less than 10 cm deep (see Fig. 3a), the depth of the bioturbated zone was taken to be the maximum depth of the Holocene layer (i.e. for $z_{\text{holo}} < 10$ cm, $z_{\text{bio}} < 10$ cm).

tive assessment of the amount of POC stored and degraded in marine sediments deposited in three dimensions over the Quaternary Period. As such, it is difficult to compare most of the results of this study to other published studies since so few of these quantities have been reported. In addition, the lack of a common reference frame can complicate comparisons of, for example, carbon burial efficiency, *BE*, with the existing literature. For instance, when values of *BE* are specified, they are nearly always based on the fraction of POC at a defined sediment depth relative to the amount arriving at the sediment water interface. This approach ignores differing sedimentation rates and thus the differing

amounts of time that POC has undergone degradation. It is illustrative to note that the age of POC in sediments one meter beneath the SWI in the South Pacific Gyre can reach one million years, while for some coastal settings, POC at the same depth could be as young as a few thousand years. Despite these obstacles, we can compare our results to some of the attempts to quantify the global organic carbon budget in marine sediments.

4.1.1. Global rates

The calculated global rates of POC degradation in marine sediments presented in this study ($1.314 \text{ Pg C yr}^{-1}$ for bioturbated Holocene sediments in the baseline scenario and $3.689 \text{ Pg C yr}^{-1}$ for the low-reactivity scenario), are similar to other global values published in the literature, though it is unclear over what sediment depth/age these values are relevant: $2.308 \text{ Pg C yr}^{-1}$ (Jørgensen, 1983), $2.616 \text{ Pg C yr}^{-1}$ (Smith and Hollibaugh, 1993), $1.991 \text{ Pg C yr}^{-1}$ (Burdige, 2007), 1.784 or $3.127 \text{ Pg C yr}^{-1}$ (Middelburg et al., 1997) and $>6 \text{ Pg C yr}^{-1}$ (Middelburg, 2019). Using O_2 consumption data, (Middelburg, 2019) estimates that sediments at 100, 200, 1000 and 2000 m water depth are responsible for consuming, respectively, 1.770, 1.590, 1.380 and $1.260 \text{ Pg C yr}^{-1}$. Our results (Table 4) show that in the baseline and low-reactivity scenarios, the integrated rates of POC degradation in all Quaternary sediments are 1.751 and $4.038 \text{ Pg C yr}^{-1}$.

We calculate that nearly 85% of POC degradation occurs in shelf sediments for bioturbated Holocene sediments in the baseline scenario, while others have reported 83% (Jørgensen, 1983) and 87% (Bernier, 1982) for shelf settings of unspecified sediment age. We also calculate that 8.6% and 0.6% of POC is degraded in abyssal sediments for the baseline and low-reactivity scenarios, while Jørgensen (1983) estimated that it is 2%, with the same caveat as for the shelf sediments.

4.1.2. Mass stored

Another quantity published in the literature that could be compared to our results is the mass of POC stored in sediments. Eglington and Repeta (2014), based on earlier

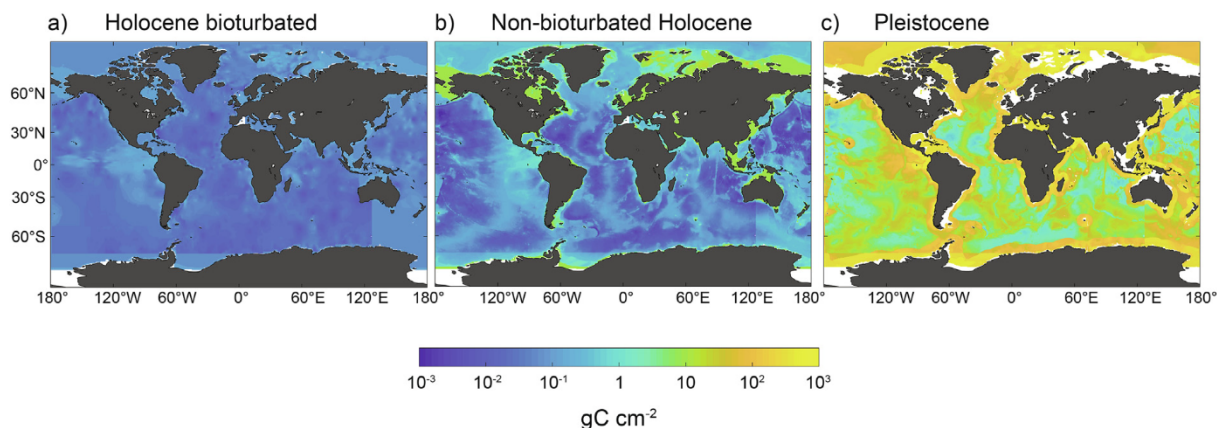


Fig. 6. Integrated masses of particulate organic carbon, POC, preserved ($\bar{P}OC$) in (a) the bioturbated Holocene, (b) non-bioturbated Holocene and (c) Pleistocene sediment layers for the baseline POC reactivity scenario.

Table 4

Rates of particulate organic carbon, POC, degradation in the bioturbated Holocene, non-bioturbated Holocene and Pleistocene layers in the baseline and low and high POC reactivity scenarios considered in this study.

Units are 10^{13} g C yr ⁻¹	Baseline	Low reactivity	High reactivity
Bioturbated Holocene Layer			
Shelf	111.2	360.2	27,893
Margin	8.35	6.68	11,500
Abyss	11.84	2.25	102.4
Total	131.4	368.9	39,490
Non-bioturbated Holocene layer			
Shelf	12.3	12.6	3.97
Margin	0.45	0.38	0.19
Abyss	0.75	0.15	0.95
Total	13.4	13.2	5.11
Pleistocene layer			
Shelf	0.01	0.01	0.002
Margin	3.89	4.31	1.08
Abyss	7.9	6.56	7.07
Total	11.81	10.88	8.15

The depth of the bioturbated layer is set to 10 cm, but the depths of the Holocene and Pleistocene layers are based on their ages and are therefore variable (see Fig. 4). For locations where the Holocene sediment layer is less than 10 cm deep (see Fig. 3a), the depth of the bioturbated zone was taken to be the maximum depth of the Holocene layer (i.e. for $z_{\text{holo}} < 10$ cm, $z_{\text{bio}} < 10$ cm).

reports (Hedges, 1992; Hedges and Oades, 1997), declared that “recent sediments” contain 1.50×10^{17} g of organic C. More recently, a machine learning approach was used to estimate that the top 5 cm of global marine sediments contain $0.87 \pm 0.45 \times 10^{17}$ g C (Lee et al., 2019). Our calculations estimate that the bioturbated Holocene layer alone contains a similar amount, 1.68×10^{17} g C (baseline scenario), but non-bioturbated Holocene sediments contain more than an order of magnitude more, 2.49×10^{18} g C. In this case, comparisons to the literature rely on the meaning of the word “recent.” By our calculations, Quaternary sediments, which could be considered recent, contain 1.46×10^{20} g C. This is about two orders of magnitude less

that the estimated total amount of organic carbon in marine sediments, 1.25×10^{22} g C (Ronov and Yaroshevskiy, 1976; Ronov, 1982), though this value is an extrapolation based on near-shore POC measurements. This mass of organic carbon translates to a global marine sediment average of 3.6 dry wt. % POC (for total volume of marine sediments of 3.01×10^{23} cm³ (LaRowe et al., 2017), a nominal porosity of 50% and sediment grain density of 2.3 g cm⁻³), a massive amount that is rarely found anywhere beyond surface sediments near land masses.

4.1.3. Burial efficiencies

Calculated burial rates/efficiencies presented in this study (0.328 Pg C yr⁻¹/20% for bioturbated Holocene sediments in the baseline scenario and 0.291 Pg C yr⁻¹/7.3% for the low-reactivity scenario) are similar to other global values published in the literature: 0.16 Pg C yr⁻¹ (Hedges and Keil, 1995), 0.309 Pg C yr⁻¹ (Burdige, 2007), 0.223 Pg C yr⁻¹ (Gershanovich et al., 1974), 0.126 Pg C yr⁻¹ (Bernier, 1989), 0.15 Pg C yr⁻¹ (Müller-Karger et al., 2005), 0.2 – 0.3 Pg C yr⁻¹ (Middelburg, 2019). Burdige (2007) converted a number of these values to global carbon BE, resulting in values ranging from 13.4% to 45.4% (neither the depth nor the age of burial is specified). Using a benthic model where POC degradation was empirically constrained using a power law, Stolpovsky et al. (2015) determined a global mean BE of 6.1 ± 3 % for bioturbated Holocene sediments. Burial efficiencies for the baseline, low and high POC reactivity scenarios in the bioturbated Holocene layer determined here are 20%, 7.3% and 0.03%. For non-bioturbated Holocene sediments, values of BE are 11.8%, 4% and 0.01% for the same three reactivity scenarios. The baseline, low and high POC reactivity scenarios yield burial efficiencies in Pleistocene sediments of 24.4%, 34% and 5.7%, respectively. Our BE results are consistent with the range reported by Burdige (2007), and similar to those of Stolpovsky et al. (2015). This is despite the fact that our model makes no explicit concessions for specific factors that can alter the preservation efficiency of POC, such as the mineralogy and surface area of inorganic sedimentary particles and oxygen exposure time, although they are implicitly accounted for in the RCM parameters *ia* and

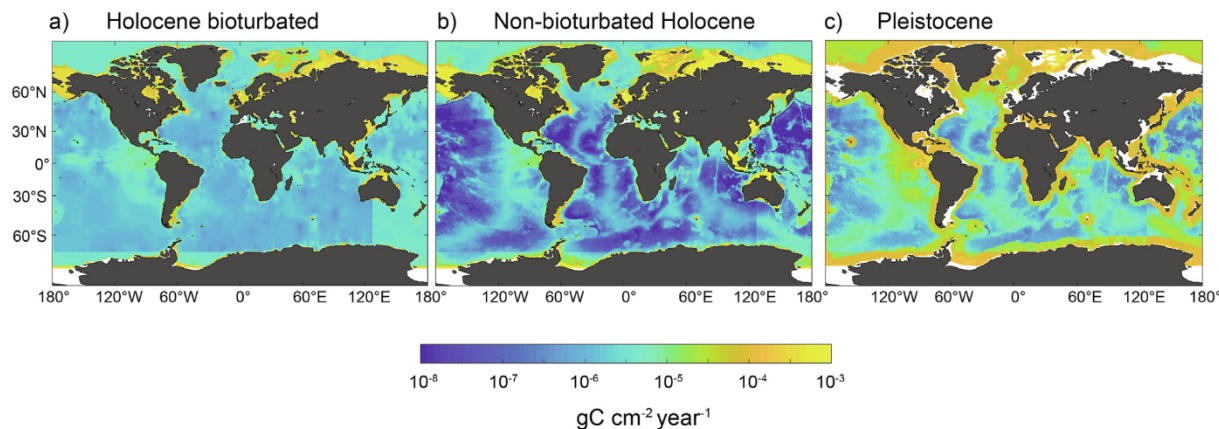


Fig. 7. Integrated rates of particulate organic carbon, POC, degradation (\bar{R}) in (a) the bioturbated Holocene, (b) non-bioturbated Holocene and (c) Pleistocene sediment layers for the baseline POC reactivity scenario.

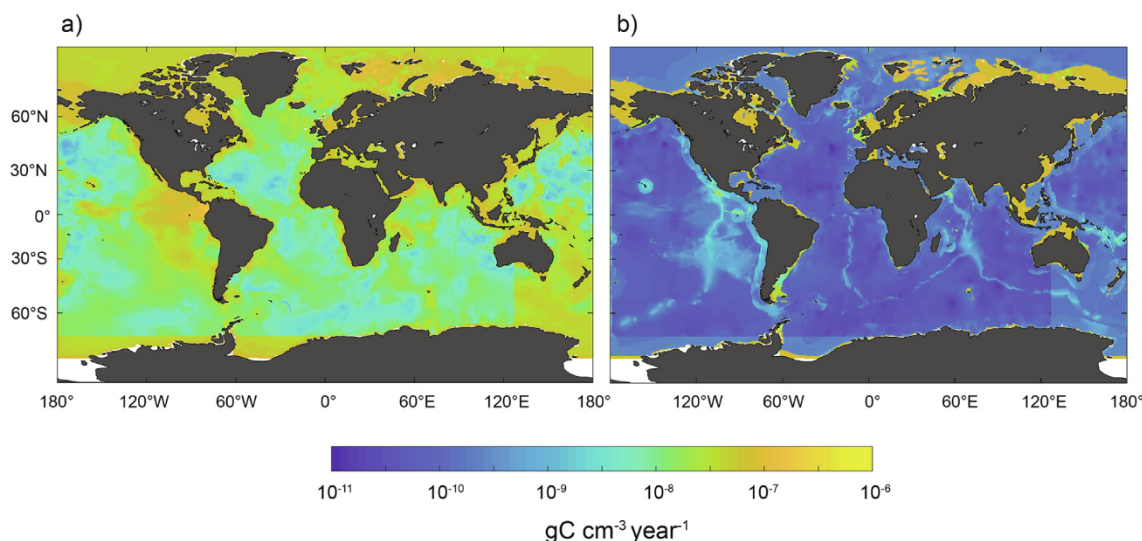


Fig. 8. Rates of particulate organic carbon, POC, degradation in sediments deposited at the beginnings of the (a) Holocene and (b) Pleistocene for the baseline POC reactivity scenario.

v (Keil et al., 1994; Mayer, 1994; Hedges et al., 1999). Most likely, the tested ranges of the POC reactivity parameter ia cover a large fraction of the uncertainty associated with these factors. We also did not consider sediment resuspension on the continental margins by currents, internal waves or mass wasting events, which can then be transported up- or downslope (Hosegood and van Haren, 2004; Martini et al., 2013).

The spatial distribution of POC degradation also compares favorably with values reported in the literature. Our BE values for margin sediments in bioturbated Holocene sediments, 18.1% and 21.8% - for the baseline and low-reactivity scenarios, respectively, are similar to the 15% reported by Jørgensen (1983) – a value that includes sediments under water depth from 200 to 4000 m, whereas our result span 200–3500 m. Similarly, we compute that 87% of POC burial occurs on the shelf and margins for the baseline bioturbated Holocene scenario, similar to the 90% reported by Hedges and Keil (1995).

4.2. Microbial degradation of organic carbon

One of the most important factors determining the size and activity level of a given microbial population is the amount of energy that is available to it and the rate at which this energy is supplied. The rate at which energy is made available in marine sediments, the microbial power supply (see LaRowe and Amend, 2015a), is largely controlled by the rate at which POC is delivered to sediments. Therefore, the rates of POC degraded in bioturbated Holocene, non-bioturbated Holocene and Pleistocene sediments (Table 4) effectively display the rates of microbial activity in sediments down to the depths shown in Fig. 4. For instance, 13.4×10^{13} g of carbon is degraded in non-bioturbated Holocene sediments per year, with the majority of it (92%) degraded in shelf sediments. By contrast, only about 6% of non-bioturbated Holocene POC degradation occurs

in abyssal sediments (see Table 4). However, in the Pleistocene layer, these trends are reversed. Furthermore, because the absolute amount of POC that is deposited on continental shelves and margins is far greater than the amount that arrives at the SWI in open ocean settings, the rates and sizes of near-shore sedimentary microbial communities should be far larger than those in the abyss. However, due to different sedimentation patterns in the Pleistocene globally (Figs. 3 and 4), more POC is degraded in abyssal sediments than margin sediments, with a much smaller amount in shelf sediments.

The average numbers of heterotrophic microbes calculated to be actively maintained through the degradation of organic carbon in the representative sediment columns shown in Fig. 9b ($\sim 10^4$ to 10^{-3} cells cm^{-3}) are many orders of magnitude lower than cell counts in marine sediments. Cell counts in surface sediments vary between at least 10^5 and 10^{10} cells cm^{-3} (Kallmeyer et al., 2012; Parkes et al., 2014; D'Hondt et al., 2015), while deeper in a given sediment column, cell numbers typically, but not always (e.g., D'Hondt et al., 2004) decrease according to a power law (Kallmeyer et al., 2012; Parkes et al., 2014). In coastal sediments tens to hundreds of meters below the SWI, cell counts are typically 10^6 – 10^8 cells cm^{-3} , while at equivalent sediment depths under oligotrophic waters, cells counts are more likely to vary between 10^3 and 10^6 cells cm^{-3} (Kallmeyer et al., 2012; D'Hondt et al., 2015). Clearly, the procedures used to estimate biomass in this study do not match reported cell counts.

The values of maintenance power, P_m , used in Eq. (18), which are derived from laboratory studies of *growing* organisms, are thought to be far larger than those of organisms living in relatively low-energy environments (Hoehler and Jørgensen, 2013). In fact, recent studies have shown that when maintenance powers that are two orders of magnitude lower than the lowest reported in the literature are used to estimate the number of microbes in very-low energy

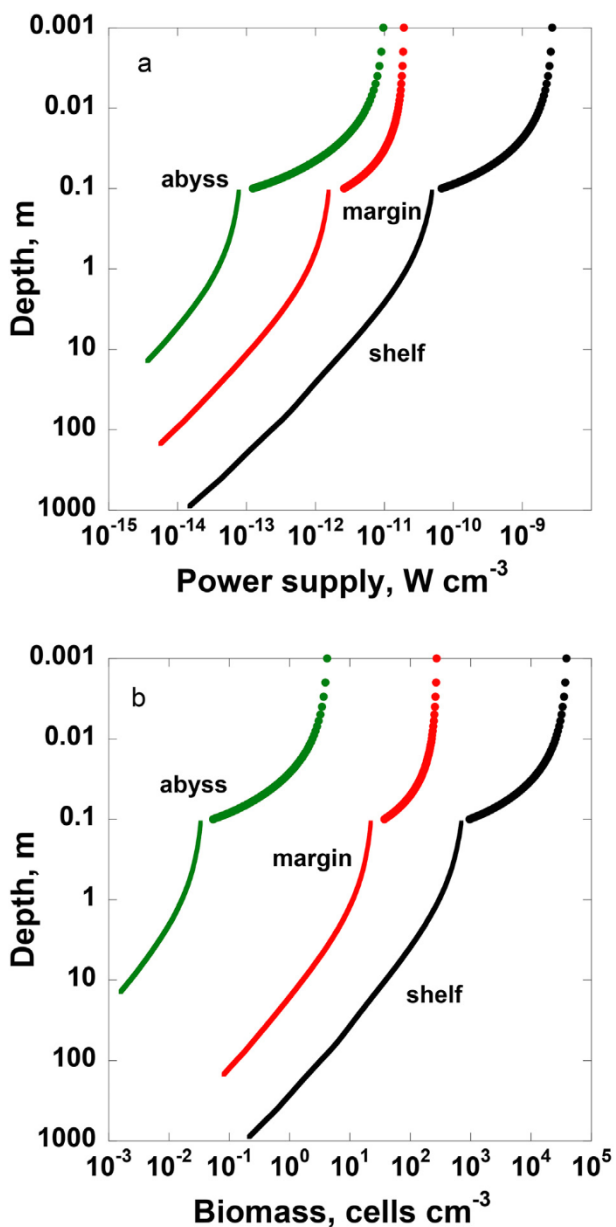


Fig. 9. (a) Power available and (b) biomass that could be supported on maintenance power from particulate organic carbon, POC, degradation in sediment columns that are representative of the shelf, margin and abyss domains. The sedimentation rates (ω), sediment water interface, SWI, porosities (ϕ_0), compaction length scales (c_0), POC reactive continuum ia and v parameters, SWI POC contents (POC_0) and bioturbation coefficients (D_b) used for these domains are given in order of shelf, margin, abyss as follows: ω (0.04, 0.006145, 0.000589 cm yr⁻¹), ϕ_0 (0.45, 0.74, 0.7), c_0 (0.0005, 0.00017, 0.00085 m⁻¹), ia (52.59, 1816, 2184 yr), v (0.125), POC_0 (2, 1, 0.5 wt%) and D_b (27.5, 5.54, 0.311 cm² yr⁻¹).

sediments, the predictions closely match cell counts (LaRowe and Amend, 2015a, b). If we used P_d values representative of natural marine sediments, which are constrained by geochemical data and modeling results (0.01 fW cell⁻¹ (LaRowe and Amend, 2015a, 2015b)), the predicted

cell abundances would be five orders of magnitude higher than those shown in Fig. 9b, which are calculated using laboratory-derived P_d values. Such estimates are much more in line with cell counts for these types of settings (Kallmeyer et al., 2012). It should be noted that this analysis does not take into account the energetics of growth and/or biomass replacement, which can vary substantially depending on environmental conditions (LaRowe and Amend, 2016). In addition, we do not attempt to account for the number of microorganisms that could be maintaining themselves via fermentation, methanogenesis or chemolithotrophy.

4.3. Deeper organic carbon

The discussion of organic carbon thus far has focused on environments for which sedimentation and organic carbon deposition rates are reasonably well-known throughout the Quaternary Period, about ~18% of the total volume of global marine sediments (LaRowe et al., 2017). That is, sediments older than 2.59 Ma have not been discussed with respect to the amount of microbial biomass contained within them, or their metabolic activity, despite the fact that microbial cells have been found in sediments far older than the Quaternary (D'Hondt et al., 2004; Kallmeyer et al., 2012; D'Hondt et al., 2015) that seem to be active or capable of activity (Schippers et al., 2005; Morono et al., 2011; Engelhardt et al., 2014; Inagaki et al., 2015). Although all three of the POC reactivity scenarios for the Pleistocene considered in this study show that a significant amount of organic carbon has been buried beneath 2.59 Myr-old sediments, the distribution and rates of organic carbon degradation beneath these depths cannot be estimated using the model described in this study without additional information extending further back into the Cenozoic Era.

Despite these limitations, evidence for variations in global organic carbon deposition over geological timescales is abundant (Bernier, 2004). Deep marine sediments have prominently recorded seven major climate and carbon cycle perturbations during the Jurassic and Cretaceous periods known as Oceanic Anoxic Events (OAEs, (Jenkyns, 2010)), intervals of enhanced global deposition of organic carbon forming black shale layers with POC contents between 2 and 30 wt%. In addition to global events, regional climate change has also enhanced organic carbon deposition in specific ocean regions. For instance, marine sediments in the Mediterranean reveal a quasi-periodic deposition of organic-carbon-rich layers, so-called sapropels, over the last 13.5 million years. Assessing the significance of these paleo-strata for the global sedimentary OC budget and energy availability in the deep biosphere is compromised by the difficulties associated with constraining the spatial and temporal distribution of organic carbon deposition during these times, as well as determining their current burial depth. However, pore water data and inverse modelling can reveal significant changes in the magnitude and quality of organic carbon deposition in some regions, e.g. Arndt et al. (2006, 2009); Wehrmann et al. (2013).

5. CONCLUDING REMARKS

In this study, we presented the most comprehensive quantitative analysis to date of the global distribution and degradation rates of particulate organic carbon in marine sediments. The results are reported in terms of ocean provinces based largely on water depth, and temporally in terms of the Holocene and Pleistocene, but the data sets and methods can be used to assess the amount of POC in marine sediments at any location or time-period (≤ 2.59 Ma). One such application of this model is the quantification of near-shore carbon stocks for maritime nations as part of climate-mitigation action (Avelar et al., 2017). More specifically, a more advanced version of the model presented here could help predict the fate of POC converted by microbial activity to CO_2 vs. CH_4 , and thus the radiative forcing power of the respired carbon. However, the more profound application of our model is what it reveals about the deep biosphere, a poorly understood but vast window into the limits of life on Earth and perhaps elsewhere.

Simply put, the relatively recent discovery of viable microorganisms deep in marine sediments has changed how scientists view the size and extent of the biosphere. Although there was already a growing consensus that these microorganisms are operating at much lower power levels than their surface analogs (e.g. Hoehler and Jørgensen, 2013; LaRowe and Amend, 2015a, 2015b), virtually nothing was known about what these organisms are doing or the rates at which they are active on a global scale. The model results presented in this study help decipher the structure and activity levels of microorganisms in the deep biosphere while revealing the spatial history of organic carbon degradation and burial throughout the Quaternary period. When expressed through a bioenergetic perspective, the rates of organic carbon degradation and burial not only compare well with other estimated values, but correspond with microbial cell densities reported in the literature when appropriately low maintenance powers are used instead of laboratory-determined ones. Instead of just knowing the number of microorganisms living in marine sediments, we can now specify the rates at which they are consuming organic carbon and where they are active. As models such as the one presented above are applied to deeper sediments, in conjunction with global-scale data on the occurrence of organic-rich horizons, a more complete descriptions of the deep biosphere and the organic carbon cycle are possible.

Declaration of Competing Interest

The authors declare that they have no known competing financial interests or personal relationships that could have appeared to influence the work reported in this paper.

ACKNOWLEDGEMENTS

This work was supported by the NSF-sponsored Center for Dark Energy Biosphere Investigations (C-DEBI) under grant OCE0939564 (DEL, JAB, JPA); NASA Astrobiology Institute — Life Underground (NAI-LU) grant NNA13AA92A (DEL, JPA); the USC Zumberge Fund Individual Grant (DEL); the Alfred P.

Sloan Foundation through the Deep Carbon Observatory (DEL, JAB); the Alexander von Humboldt Foundation (JAB); NERC NE/T010967/1 (JAB); the European Union Horizon 2020 research and innovation program under the Marie Skłodowska-Curie grant agreement no. 643052 (C-CASCADES) (SA) and the NASA-NSF Origins of Life Ideas Lab program under grant NNN13D466T (DEL). This is C-DEBI contribution 538 and NAI-LU contribution 143.

APPENDIX A

The rate of POC degradation in bioturbated sediments has been approximated with a 500-G model in which the amount and reactivity of POC in each pool is determined using the same framework as the Reactive Continuum Model (Eq. (3)). This is done because the age of POC in bioturbated sediments, a parameter required to use the RCM, is not well-constrained (Meile and Van Cappellen, 2005). This means that within the bioturbated zone, POC is represented by 500 distinct fractions that are degraded according to a first-order organic carbon degradation rate law:

$$R_{POC} = \sum_{i=1}^{500} k_i \cdot POC_i(z) \quad (\text{A.1})$$

where k_i is the rate constant and

$$POC_i(0) = F_i \cdot POC \quad (\text{A.2})$$

The initial proportion of total organic carbon in fraction i , F_i , as well as its respective reactivity, k_i , can be determined through the initial probability density function that determines the concentration of organic carbon having a degradability between k and $k + dk$ at time 0 (Eq. (3)). The initial fraction of total POC characterized by a distinct reactivity k is given by:

$$f(k, 0) = \frac{om(k, 0)}{POC_0} = \frac{ia^v \cdot k^{v-1} \cdot e^{-ia \cdot k}}{\Gamma(v)} \quad (\text{A.3})$$

The initial fraction of POC within the reactivity range between 0 and k , i.e., having a reactivity $\leq k$, is then given by integrating Eq. (A.3), assuming $ia, v, k > 0$:

$$\begin{aligned} F(k, 0) &= \int_0^k f(0, k) dk = \int_0^k \frac{ia^v \cdot k^{v-1} \cdot e^{-ia \cdot k}}{\Gamma(v)} dk = \\ &= \frac{ia^v \cdot k^v \cdot (ia \cdot k)^{-v} (\Gamma(v) - \Gamma(v, ia \cdot k))}{\Gamma(v)} \\ &= \left(\frac{1 - \Gamma(v, ia \cdot k)}{\Gamma(v)} \right) \end{aligned} \quad (\text{A.4})$$

where $\Gamma(v, ia \cdot k)$ denotes the inverse gamma function.

In the bioturbated sediment layer, the RCM was approximated by dividing the reactivity range $k = [10^{-15}, 10^{(-\log(ia) + 2)}]$ into 500 equal reactivity bins, k_j , thus ensuring a comprehensive approximation of the gamma function defined by the respective ia and v values. The initial fraction, F_i , of total POC within the reactivity bin k_{j-1} and k_j (and thus with reactivity $k_i = k_{j-1} + (k_j - k_{j-1})/2$) in the 500G model can then be calculated as:

$$F_i = F(k_j, 0) - F(k_{j-1}, 0) \quad (\text{A.5})$$

The most reactive fraction, F_{500} , with reactivity $k_{500} = 10^{-\log(ia) + 2} \text{ yr}^{-1}$ was calculated on the basis of the upper incomplete gamma function:

$$F_{500} = \int_{k_{500}}^{\infty} f(k_{500}, 0) dk = \frac{\Gamma(v, ia \cdot k_{500})}{\Gamma(v)} \quad (\text{A.6})$$

For the bioturbated Holocene layer, the depth dependence of k is given by

$$k(z) = \sum_i k_i \cdot \left(\frac{POC_i(z)}{POC(z)} \right) \quad (\text{A.7})$$

which is a close approximation of how $k(z)$ is calculated for the nonbioturbated sediment layers, i.e.

$$k(z) = \frac{v}{ai + age(z)} \quad (\text{A.8})$$

The derived rate constants were then used in Eq. (1) by expressing R_{POC} according to Eq. (5) to determine POC concentrations and degradation rates in the bioturbated Holocene layer ($< z_{bio}$). For this purpose, Eq. (1) was solved analytically. Assuming steady state conditions and constant values of D_b , ω and ϕ for a given location and depth, the general solution of Eq. (1) for each organic carbon fraction i is given by:

$$POC_i(z) = A_i e^{(a_i z)} + B_i e^{(b_i z)} \quad (\text{A.9})$$

where

$$a_i = \frac{\omega - \sqrt{\omega^2 + 4D_b \cdot k_i}}{2D_b} \quad (\text{A.10})$$

$$b_i = \frac{\omega + \sqrt{\omega^2 + 4D_b \cdot k_i}}{2D_b} \quad (\text{A.11})$$

and

$$POC(z) = \sum_{i=1}^{500} POC_i(z) \quad (\text{A.12})$$

The integration constants A_i and B_i are defined by the chosen boundary conditions. Here, we apply a known concentration at the sediment-water interface ($POC(0) = POC_0$) and assume continuity (equal flux and concentration) across the bottom of the bioturbated layer ($POC(z_{bio}) = POC_{z_{bio}}; \left. \frac{-D_b dPOC}{dz} \right|_{z_{bio}} = 0$).

REFERENCES

- Amend J. P. and LaRowe D. E. (2019) Minireview: demystifying microbial reaction energetics. *Environ. Microbiol.* **21**, 3539–3547.
- Archer D. E., Morford J. L. and Emerson S. R. (2002) A model of suboxic sedimentary diagenesis suitable for automatic tuning and gridded global domains. *Global Biogeochem. Cycles* **16**, 1017. <https://doi.org/10.1029/2000GB001288>.
- Aris R. (1968) Prolegomena to the rational analysis of systems of chemical reactions, II. Some adenda. *Arch. Rational Mech. Anal.* **27**, 356–364.
- Arndt S., Brumsack H.-J. and Wirtz K. W. (2006) Cretaceous black shales as active bioreactors: a biogeochemical model for the deep biosphere encountered during ODP Leg 207 (Demerara Rise). *Geochim. Cosmochim. Acta* **70**, 408–425.
- Arndt S., Hetzel A. and Brumsack H.-J. (2009) Evolution of organic matter degradation in Cretaceous black shales inferred from authigenic barite: a reaction-transport model. *Geochim. Cosmochim. Acta* **73**, 2000–2022.
- Arndt S., Jørgensen B. B., LaRowe D. E., Middelburg J. B. M., Pancost R. D. and Regnier P. (2013) Quantifying the degradation of organic matter in marine sediments: a review and synthesis. *Earth Sci. Rev.* **123**, 53–86.
- Athy L. F. (1930) Density, porosity and compaction of sedimentary rocks. *AAPG Bull.* **14**, 1–24.
- Avelar S., van der Voort T. S. and Eglinton T. I. (2017) Relevance of carbon stocks of marine sediments for national greenhouse gas inventories of maritime nations. *Carbon Balance Manage.* **12**. <https://doi.org/10.1186/s13021-13017-10077-x>.
- Berner B. A. (1989) Biogeochemical cycles of carbon and sulfur and their effect on atmospheric oxygen over Phanerozoic time. *Palaeogeog. Palaeoclim. Palaeoecol.* **75**, 97–122.
- Berner R. A. (1980) *Early Diagenesis: A Theoretical Approach*. Princeton Univ. Press, Princeton, N.J..
- Berner R. A. (1982) Burial of organic carbon and pyrite sulfur in the modern ocean; its geochemical and environmental significance. *Am. J. Sci.* **282**, 451–473.
- Berner R. A. (2004) *The Phanerozoic Carbon Cycle: CO₂ and O₂*. Oxford University Press, Oxford.
- Berner R. A. (2006) GEOCARBSULF: A combine model for Phanerozoic atmospheric O₂ and CO₂. *Geochim. Cosmochim. Acta* **70**, 5653–5664.
- Betts J. N. and Holland H. D. (1991) The oxygen content of ocean bottom waters, the burial efficiency of organic carbon, and the regulation of atmospheric oxygen. *Palaeogeog. Palaeoclim. Palaeoecol.* **97**, 5–18.
- Boudreau B. P. (1994) Is burial velocity a master parameter for bioturbation? *Geochim. Cosmochim. Acta* **58**, 1243–1249.
- Boudreau B. P. (1997) *Diagenetic Models and their Implementation: Modelling Transport and Reactions in Aquatic Sediments*. Springer, Berlin.
- Boudreau B. P., Arnosti C., Jørgensen B. B. and Canfield D. E. (2008) Comment on “Physical Model for the Decay and Preservation of Marine Organic Carbon”. *Science* **319**, 1616.
- Boudreau B. P. and Ruddick B. R. (1991) On a reactive continuum representation of organic matter diagenesis. *Am. J. Sci.* **291**, 507–538.
- Bradley J. A., Amend J. P. and LaRowe D. E. (2018a) Bioenergetic controls on microbial ecophysiology in marine sediments. *Front. Microbiol.* **9**, 180.
- Bradley J. A., Amend J. P. and LaRowe D. E. (2018b) Necromass as a limited source of energy for microorganisms in marine sediments. *J. Geophys. Res. Biogeosci.* **123**, 577–590.
- Bradley J. A., Amend J. P. and LaRowe D. E. (2019) Survival of the fewest: microbial dormancy and maintenance in marine sediments through deep time. *Geobiology* **17**, 43–59.
- Burdige D. J. (2007) Preservation of organic matter in marine sediments: controls, mechanisms and an imbalance in sediment organic carbon budgets? *Chem. Rev.* **107**, 467–485.
- Burwicz E. B., Rüpke L. H. and Wallmann K. (2011) Estimation of the global amount of submarine gas hydrates formed via microbial methane formation based on numerical reaction-transport modeling and a novel parameterization of Holocene sedimentation. *Geochim. Cosmochim. Acta* **75**, 4562–4576.
- Canfield D. E. (1993) Organic matter oxidation in marine sediments. In *Interactions of C, N, P and S Biogeochemical Cycles and Global Change* (eds. R. Wollast, F. T. MacKenzie and L. Chou). Springer-Verlag, Berlin, pp. 333–363.

- Canfield D. E., Kristensen E. and Thamdrup B. (2005) *Advances in Marine Biology: Aquatic Geomicrobiology*. Elsevier Academic Press, San Diego.
- Colman A. S. and Holland H. D. (2000) The global diagenetic flux of phosphorous from marine sediments to the ocean: redox sensitivity and the control of atmospheric oxygen levels. *Marine Authigenesis: From Global to Microbial*. Society of Sedimentary Geology.
- D'Hondt S., Inagaki F., Zarikian C. A., Abrams L. J., Dubois N., Engelhardt T., Evans H., Ferdelman T., Gribsholt B., Harris R., Hoppie B. W., Hyun J.-H., Kallmeyer J., Kim J., Lynch J. E., McKinley C. C., Mitsunobu S., Morono Y., Murray R. W., Pockalny R., Sauvage J., Shimono T., Shiraiishi F., Smith D. C., Smith-Duque C. E., Spivack A. J., Steinsbu B. O., Suzuki Y., Szpak M., Toffin L., Uramoto G., Yamaguchi Y. T., Zhang G., Zhang X.-H. and Ziebis W. (2015) Presence of oxygen and aerobic communities from sea floor to basement in deep-sea sediments. *Nat. Geosci.* **8**, 299–304.
- D'Hondt S., Jørgensen B. B., Miller D. J., Batzke A., Blake R., Cragg B. A., Cypionka H., Dickens G. R., Ferdelman T., Hinrichs K. U., Holm N. G., Mitterer R., Spivack A., Wang G. Z., Bekins B., Engelen B., Ford K., Gettemy G., Rutherford S. D., Sass H., Skilbeck C. G., Aiello I. W., Guerin G., House C. H., Inagaki F., Meister P., Naehr T., Niitsuma S., Parkes R. J., Schippers A., Smith D. C., Teske A., Wiegel J., Padilla C. N. and Acosta J. L. S. (2004) Distributions of microbial activities in deep seafloor sediments. *Science* **306**, 2216–2221.
- Dale A. W., Boyle R. A., Lenton T. M., Ingall E. D. and Wallmann K. (2016) A model for microbial phosphorus cycling in bioturbated marine sediments: significance for phosphorus burial in the early Paleozoic. *Geochim. Cosmochim. Acta* **189**, 251–268.
- Dale A. W., Nickelsen L., Scholz F., Hensen C., Oschlies A. and Wallmann K. (2015) A revised global estimate of dissolved iron fluxes from marine sediments. *Global Biogeochem. Cycles* **29**, 691–707.
- Eakins B. W. and Sharman G. F. (2010) *Volumes of the World's Oceans from ETOPO1*. NOAA National Geophysical Data Center, Boulder CO.
- Eglinton T. I. and Repeta D. J. (2014) Organic matter in the contemporary ocean. In *Treatise on Geochemistry* (eds. K. K. Turekian and H. D. Holland), second ed. Elsevier, Amsterdam, pp. 151–189.
- Emerson S. and Bender M. (1981) Carbon fluxes at the sediment-water interface of the deep-sea – calcium carbonate preservation. *J. Mar. Res.* **39**, 139–162.
- Engelhardt T., Kallmeyer J., Cypionka H. and Engelen B. (2014) High virus-to-cell ratios indicate ongoing production of viruses in deep subsurface sediments. *ISME J.* **8**, 1503–1509.
- Freitas F. S., Pancost R. D. and Arndt S. (2017) The impact of alkenone degradation on $U^{K^{37}}$ paleothermometry: a model-derived assessment. *Paleoceanography* **32**, 648–672.
- Gershanovich D. E., Gorshkova T. I. and Koniukhov I. (1974) Organic matter in recent and fossil sediments and methods of its investigation. Nauka, Moscow.
- Glombitza C., Jaussi M. and Røy H. (2015) Formate, acetate, and propionate as substrates for sulfate reduction in sub-arctic sediments of Southwest Greenland. *Front. Microbiol.* **6**, 846.
- Hantschel T. and Kauerauf A. I. (2009) *Fundamentals of Basin and Petroleum Systems Modeling*. Springer-Verlag, Berlin.
- Hay W. W. (1994) Pleistocene-Holocene fluxes are not the Earth's norm. In *Material Fluxes on the Surface of the Earth* (eds. W. W. Hay and T. Usselman). National Academy Press, Washington D.C., pp. 15–27.
- Hedges J. I. (1992) Global biogeochemical cycles: progress and problems. *Mar. Chem.* **39**, 67–93.
- Hedges J. I., Hu F. S., Devol A. H., Hartnett H. E., Tsamakis E. and Keil R. G. (1999) Sedimentary organic matter preservation: a test for selective degradation under oxic conditions. *Am. J. Sci.* **299**, 529–555.
- Hedges J. I. and Keil R. G. (1995) Sedimentary organic matter preservation: an assessment and speculative hypothesis. *Mar. Chem.* **49**, 81–115.
- Hedges J. I. and Oades J. M. (1997) Comparative organic geochemistries of soils and marine sediments. *Org. Geochem.* **27**, 319–361.
- Helgeson H. C. (1969) Thermodynamics of hydrothermal systems at elevated temperatures and pressures. *Am. J. Sci.* **267**, 729–804.
- Helgeson H. C., Kirkham D. H. and Flowers G. C. (1981) Theoretical prediction of thermodynamic behavior of aqueous electrolytes at high pressures and temperatures: 4. Calculation of activity coefficients, osmotic coefficients, and apparent molal and standard and relative partial molal properties to 600°C and 5 kb. *Am. J. Sci.* **281**, 1249–1516.
- Ho T. C. and Aris R. (1987) On apparent second-order kinetics. *Amer. Inst. Chem. Eng. J.* **33**, 1050–1051.
- Hoehler T. M. and Jørgensen B. B. (2013) Microbial life under extreme energy limitation. *Nat. Rev. Microbiol.* **11**, 83–94.
- Hosegood P. and van Haren H. (2004) Near-bed solibores over the continental slope in the Faeroe-Shetland Channel. *Deep-Sea Res. II* **51**, 2943–2971.
- Inagaki F., Hinrichs K.-U., Kubo Y., Bowles M. W., Heuer V. B., Hong W.-L., Hoshino T., Ijiri A., Imachi H., Ito M., Kaneko M., Lever M. A., Lin Y.-S., Methé B. A., Morita S., Morono Y., Tanikawa W., Bihan M., Bowden S. A., Elvert M., Glombitza C., Gross D., Harrington G. J., Hori T., Li K., Limmer D., Liu C.-H., Murayama M., Ohkouchi N., Ono S., Park Y.-S., Phillips S. C., Prieto-Mollar X., Purkey M., Riedinger N., Sanada Y., Sauvage J., Snyder G., Susilawati R., Takano Y., Tasumi E., Terada T., Tomaru H., Trembath-Reichert E., Wang D. T. and Yamada Y. (2015) Exploring deep microbial life in coal-bearing sediment down to ~2.5 km below the ocean floor. *Science* **349**, 420–424.
- Jenkyns H. C. (2010) Geochemistry of oceanic anoxic events. *Geochem. Geophys. Geosys.* **11**, Q03004. <https://doi.org/10.1029/202009GC002788>.
- Johnson J. W., Oelkers E. H. and Helgeson H. C. (1992) SUPCRT92 - A software package for calculating the standard molal thermodynamic properties of minerals, gases, aqueous species, and reactions from 1 bar to 5000 bar and 0°C to 1000°C. *Comput. Geosci.* **18**, 899–947.
- Jørgensen B. B. (1983) Processes at the sediment-water interface. In *The Major Biogeochemical Cycles and their Interactions* (eds. B. Bolin and R. B. Cook). J. Wiley and Sons, New York, pp. 477–515.
- Jørgensen B. B. and Kasten S. (2006) Sulfur cycling and methane oxidation. In *Marine Geochemistry* (eds. H. D. Schulz and M. Zabel), second ed. Springer, Berlin, pp. 271–308.
- Kallmeyer J., Pockalny R., Adhikari R. R., Smith D. C. and D'Hondt S. (2012) Global distribution of microbial abundance and biomass in seafloor sediment. *PNAS* **109**, 16213–16216.
- Keil R. G., Montlucon D. B., Prah F. G. and Hedges J. I. (1994) Sorptive preservation of labile organic matter in marine sediments. *Nature* **370**, 549–552.
- Lamb R. M., Harding R., Huuse M., Stewart M. and Brocklehurst S. H. (2018) The early Quaternary North Sea Basin. *Journal of the Geological Society* **175**, 275.

- LaRowe D. E. and Van Cappellen P. (2011) Degradation of natural organic matter: A thermodynamic analysis. *Geochim. Cosmochim. Acta* **75**, 2030–2042.
- LaRowe D. E. and Amend J. P. (2015a) Catabolic rates, population sizes and doubling/replacement times of microorganisms in the natural settings. *Am. J. Sci.* **315**, 167–203.
- LaRowe D. E. and Amend J. P. (2015b) Power limits for microbial life. *Front. Extr. Microbiol.* **6**, 718.
- LaRowe D. E. and Amend J. P. (2016) The energetics of anabolism in natural settings. *ISME J.* **10**, 1285–1295.
- LaRowe D. E., Arndt S., Bradley J. A., Estes E. R., Hoarfrost A., Lang S. Q., Lloyd K. G., Mahmoudi N., Orsi W. D., Shah Walter S. R., Steen A. D. and Zhao R. (2020) The fate of organic carbon in marine sediments – new insights from recent data and analysis. *Earth Sci. Rev.* **204**, 103–146.
- LaRowe D. E., Burwicz E. B., Arndt S., Dale A. W. and Amend J. P. (2017) The temperature and volume of global marine sediments. *Geology* **45**, 275–278.
- Lee T. R., Wood W. T. and Phrampus B. J. (2019) A machine learning (kNN) approach to predicting global seafloor total organic carbon. *Global Biogeochem. Cycles* **33**, 37–46.
- Lisitzin A. P. (1996) *Oceanic Sedimentation: Lithology and Geochemistry*. American Geophysical Union, Washington D. C.
- Ludwig W., Amiotte-Suchet P. and Probst J. L. (1999) Enhanced chemical weathering of rocks during the last glacial maximum: a sink for atmospheric CO₂? *Chem. Geol.* **159**, 147–161.
- Marquardt M., Hensen C., Piñero E., Wallmann K. and Haeckel M. (2010) A transfer function for the prediction of gas hydrate inventories in marine sediments. *Biogeosciences* **7**, 2925–2941.
- Martini K. I., Alford M. H., Kunze E., Kelly S. M. and Nash J. D. (2013) Internal bores and breaking internal tides on the Oregon continental slope. *J. Phys. Oceanogr.* **43**, 120–139.
- Mayer L. M. (1994) Surface area control of organic carbon accumulation in continental shelf sediments. *Geochim. Cosmochim. Acta* **58**, 1271–1284.
- Meile C. and Van Cappellen P. (2005) Particle age distributions and O₂ exposure times: timescales in bioturbated sediments. *Global Biogeochem. Cycles* **19** GB3013.
- Menard H. W. and Smith S. M. (1966) Hypsometry of ocean basin provinces. *J. Geophys. Res.* **71**, 4305–4325.
- Middelburg J. J. (1989) A simple rate model for organic matter decomposition in marine sediments. *Geochem. Cosmochim. Acta* **53**, 1577–1581.
- Middelburg J. J. (2011) Chemoautotrophy in the ocean. *Geophys. Res. Lett.* **38**.
- Middelburg J. J. (2018) Reviews and syntheses: to the bottom of carbon processing at the seafloor. *Biogeosciences* **15**, 413–427.
- Middelburg J. J. (2019) Marine carbon biogeochemistry: a primer for earth system scientists. In (eds. G. Lohmann, L. A. Mysak, J. Notholt, J. Rabassa and V. Unnithan). SpringerOpen, Cham, Switzerland, p. 118.
- Middelburg J. J., Soetaert K. and Herman M. J. H. (1997) Empirical relationships for use in global diagenetic models. *Deep-Sea Res. I* **44**, 327–344.
- Mogollón J. M., Dale A. W., Fossing H. and Regnier P. (2012) Timescales for the development of methanogenesis and free gas layers in recently-deposited sediments of Arkona Bason (Baltic Sea). *Biogeosciences* **9**, 1915–1933.
- Morono Y., Terada T., Nishizawa M., Ito M., Hillion F., Takahata N., Sano Y. and Inagaki F. (2011) Carbon and nitrogen assimilation in deep seafloor microbial cells. *PNAS* **108**, 18295–18300.
- Müller-Karger F. E., Varela R., Thunell R., Luerssen R., Hu C. and Walsh J. J. (2005) The importance of continental margins in the global carbon cycle. *Geophys. Res. Lett.* **32**, L01602.
- Parkes R. J., Cragg B., Roussel E., Webster G., Weightman A. and Sass H. (2014) A review of prokaryotic populations and processes in sub-seafloor sediments, including biosphere: geosphere interactions. *Mar. Geol.* **352**, 409–425.
- Peltier W. R. (1994) Ice age paleotopography. *Science* **265**, 195–201.
- Rohling E. J., Fenton M., Jorissen F. J., Bertrand P., Ganssen G. and Caulet J. P. (1998) Magnitudes of sea-level lowstands of the past 500,000 years. *Nature* **394**, 162–165.
- Romankevich E. A., Vetrov A. A. and Peresyppkin V. I. (2009) Organic matter of the world ocean. *Russ. Geol. Geophys.* **50**, 299–307.
- Ronov A. B. (1982) The Earth's sedimentary shell. *Int. Geol. Rev.* **24**, 1313–1388.
- Ronov A. B. and Yaroshevskiy A. A. (1976) A new model for the chemical structure of the Earth's crust. *Geochem. Int.* **13**, 89–121.
- Rothman D. H. (2002) Atmospheric carbon dioxide levels for the last 500 million years. *PNAS* **99**, 4167–4171.
- Røy H., Kallmeyer J., Adhikari R. R., Pockalny R., Jørgensen B. B. and D'Hondt S. (2012) Aerobic microbial respiration in 86-million-year-old deep-sea red clay. *Science* **336**, 922–925.
- Schippers A., Neretin L. N., Kallmeyer J., Ferdelman T. G., Cragg B. A., Parkes R. J. and Jørgensen B. B. (2005) Prokaryotic cells of the deep sub-seafloor biosphere identified as living bacteria. *Nature* **433**, 861–864.
- Schulte M. D., Shock E. L. and Wood R. (2001) The temperature dependence of the standard-state thermodynamic properties of aqueous nonelectrolytes. *Geochim. Cosmochim. Acta* **65**, 3919–3930.
- Seiter K., Hensen C., Schroter J. and Zabel M. (2004) Organic carbon content in surface sediments – defining regional provinces. *Deep-Sea Res. I* **51**, 2001–2026.
- Shock E. L. and Helgeson H. C. (1988) Calculation of the thermodynamic and transport properties of aqueous species at high pressures and temperatures – correlation algorithms for ionic species and equation of state predictions to 5 kb and 1000°C. *Geochim. Cosmochim. Acta* **52**, 2009–2036.
- Shock E. L. and Helgeson H. C. (1990) Calculation of the thermodynamic and transport properties of aqueous species at high pressures and temperatures – standard partial molal properties of organic species. *Geochim. Cosmochim. Acta* **54**, 915–945.
- Shock E. L., Helgeson H. C. and Sverjensky D. (1989) Calculation of the thermodynamic and transport properties of aqueous species at high pressures and temperatures – standard partial molal properties of inorganic neutral species. *Geochim. Cosmochim. Acta* **53**, 2157–2183.
- Shock E. L., Oelkers E., Johnson J., Sverjensky D. and Helgeson H. C. (1992) Calculation of the thermodynamic properties of aqueous species at high pressures and temperatures – effective electrostatic radii, dissociation constants and standard partial molal properties to 1000°C and 5 kbar. *J. Chem. Soc. Faraday Trans.* **88**, 803–826.
- Smith S. V. and Hollibaugh J. T. (1993) Coastal metabolism and the oceanic organic carbon balance. *Rev. Geophys.* **31**.
- Solan M., Ward E. R., White E. L., Hibberd E. E., Cassidy C., Schuster J. M., Hale R. and Godbold J. A. (2019) Worldwide measurements of bioturbation intensity, ventilation rate, and the mixing depth of marine sediments. *Sci. Data* **6**, 58.
- Stolpovsky K., Dale A. W. and Wallmann K. (2015) Toward a parameterization of global-scale organic carbon mineralization kinetics in surface marine sediments. *Global Biogeochem. Cycles* **29**, 812–829.
- Stolpovsky K., Dale A. W. and Wallmann K. (2018) A new look at the multi-H model for organic carbon degradation in surface

- marine sediments for coupled benthic-pelagic simulations of the global ocean. *Biogeosciences* **15**, 3391–3407.
- Sverjensky D., Shock E. L. and Helgeson H. C. (1997) Prediction of the thermodynamic properties of aqueous metal complexes to 1000°C and 5 kb. *Geochim. Cosmochim. Acta* **61**, 1359–1412.
- Sweetman A. K., Thurber A. R., Smith C. R., Levin L. A., Mora L. A., Wei C., Gooday A. J., Jones D. O. B., Yasuhara R. M., Ingels M., Ruhl H. A., Frieder C. A., Danovaro R., Würzberg L., Baco A., Grupe B. M., Pasulka A., Meyer K. S., Dunlop K. M., Henry L. and Roberts J. M. (2017) Major impacts of climate change on deep-sea benthic ecosystems. *Elementa: Sci. Anthropocene* **5**. <https://doi.org/10.1525/elementa.1203>.
- Tanger J. C. and Helgeson H. C. (1988) Calculation of the thermodynamic and transport properties of aqueous species at high pressures and temperatures – revised equations of state for the standard partial molal properties of ions and electrolytes. *Am. J. Sci.* **288**, 19–98.
- Thullner M., Dale A. W. and Regnier P. (2009) Global-scale quantification of mineralization pathways in marine sediments: a reaction-transport modeling approach. *Geochem. Geophys. Geosys.* **10**, 1–24.
- Tromp T. K., Van Cappellen P. and Key R. M. (1995) A global model for the early diagenesis of organic carbon and organic phosphorous in marine sediments. *Geochim. Cosmochim. Acta* **59**, 1259–1284.
- Veuger B., van Oevelen D. and Middelburg J. J. (2012) Fate of microbial nitrogen, carbon, hydrolysable amino acids, monosaccharides, and fatty acids in sediment. *Geochim. Cosmochim. Acta* **83**, 217–233.
- Vion, A. and Menot, L. (2009) Continental margins between 140m and 3500m depth. <http://www.marineregions.org/IFREMER>.
- Wadham J. L., De'Ath R., Monteiro F. M., Tranter M., Ridgwell A., Raiswell R. and Tulaczyk S. (2013) The potential role of the Antarctic Ice Sheet in global biogeochemical cycles. *Earth Environ. Sci. Trans. R. Soc. Edinburgh* **104**, 55–67.
- Walker J. C. G., Hays P. B. and Kasting J. F. (1981) A negative feedback mechanism for the long-term stabilization of Earth's surface temperature. *J. Geophys. Res.* **86**, 9776–9782.
- Wallmann K., Aloisi G., Haeckel M., Obzhairov A., Pavlova G. and Tishchenko P. (2006) Kinetics of organic matter degradation, microbial methane generation, and gas hydrate formation in anoxic marine sediments. *Geochim. Cosmochim. Acta* **70**, 3905–3927.
- Wallmann K., Pinero E., Burwicz E. B., Haeckel M., Hensen C., Dale A. W. and Ruppel L. (2012) The global inventory of methane hydrate in marine sediments: a theoretical approach. *Energies* **5**, 2449–2498.
- Wehrmann L. M., Arndt S., März C., Ferdelman T. G. and Brunner B. (2013) The evolution of early diagenetic signals in Bering Sea seafloor sediments in response to varying organic carbon deposition over the last 4.3 Ma. *Geochim. Cosmochim. Acta* **109**, 175–196.
- Westrich J. T. and Berner R. A. (1984) The role of sedimentary organic matter in bacterial sulfate reduction: the G model tested. *Limnol. Oceanogr.* **29**, 236–249.
- Zonneveld K. A. F., Versteegh G. J. M., Kasten S., Eglinton T. I., Emeis K.-C., Huguet C., Koch B. P., de Lange G. J., de Leeuw J. W., Middelburg J. J., Mollenhauer G., Prahl F. G., Rethemeyer J. and Wakeham S. G. (2010) Selective preservation of organic matter in marine environments; processes and impact on the sedimentary record. *Biogeosciences* **7**, 473–511.

Associate editor: Sabine Kasten